# Development and initial application of the global-through-urban weather research and forecasting model with chemistry (GU-WRF/Chem)

Yang Zhang,[1,2] Prakash Karamchandani,[3,4] Timothy Glotfelty,[1] David G. Streets,[5] Georg Grell,[6] Athanasios Nenes,[7,8] Fangqun Yu,[9] and Ralf Bennartz[10]

Received 19 April 2012; revised 13 August 2012; accepted 27 August 2012; published 31 October 2012.

[1] A unified model framework with online-coupled meteorology and chemistry and consistent model treatments across spatial scales is required to realistically simulate chemistry-aerosol-cloud-radiation-precipitation-climate interactions. In this work, a global-through-urban WRF/Chem model (i.e., GU-WRF/Chem) has been developed to provide such a unified model framework to simulate these important interactions across a wide range of spatial scales while reducing uncertainties from the use of offline-coupled model systems with inconsistent model treatments. Evaluation against available observations shows that GU-WRF/Chem is capable of reproducing observations with comparable or superior fidelity than existing mesoscale models. The net effect of atmospheric aerosols is to decrease shortwave and longwave radiation, $NO_2$ photolysis rate, near-surface temperature, wind speed at 10-m, planetary boundary layer height, and precipitation as well as to increase relative humidity at 2-m, aerosol optical depths, column cloud condensation nuclei, cloud optical thickness, and cloud droplet number concentrations at all scales. As expected, such feedbacks also change the abundance and lifetimes of chemical species through changing radiation, atmospheric stability, and the rates of many meteorologically-dependent chemical and microphysical processes. The use of higher resolutions in progressively nested domains from the global to local scale notably improves the model performance of some model predictions (especially for chemical predictions) and also captures spatial variability of aerosol feedbacks that cannot be simulated at a coarser grid resolution. Simulated aerosol, radiation, and cloud properties exhibit small-to-high sensitivity to various nucleation and aerosol activation parameterizations. Representing one of the few unified global-through-urban models, GU-WRF/Chem can be applied to simulate air quality and its interactions with meteorology and climate and to quantify the impact of global change on urban/regional air quality across various spatial scales.

**Citation:** Zhang, Y., P. Karamchandani, T. Glotfelty, D. G. Streets, G. Grell, A. Nenes, F. Yu, and R. Bennartz (2012), Development and initial application of the global-through-urban weather research and forecasting model with chemistry (GU-WRF/Chem), *J. Geophys. Res.*, *117*, D20206, doi:10.1029/2012JD017966.

## 1. Introduction

[2] Global change is driven by an interwoven system of human and natural processes and include both human-induced and biophysical transformations of land (e.g., urbanization, land use change, desertification), oceans (e.g., rise in sea level), atmosphere (e.g., changes in atmospheric emissions and climate), and ecosystems (e.g., migration and extinction of species). A changing climate affects air quality through a number of processes including (1) changes in

[1]Department of Marine, Earth, and Atmospheric Sciences, North Carolina State University, Raleigh, North Carolina, USA.
[2]School of Environment, Tsinghua University, Beijing, China.
[3]ENVIRON International Corporation, Novato, California, USA.
[4]Previously at Atmospheric and Environmental Research, Inc., San Ramon, California, USA.

Corresponding author: Y. Zhang, Department of Marine, Earth, and Atmospheric Sciences, North Carolina State University, Campus Box 8208, Raleigh, NC 27695, USA. (yang_zhang@ncsu.edu)

©2012. American Geophysical Union. All Rights Reserved.
0148-0227/12/2012JD017966

[5]Decision and Information Sciences Division, Argonne National Laboratory, Argonne, Illinois, USA.
[6]Earth Systems Research Laboratory, NOAA, Boulder, Colorado, USA.
[7]School of Earth and Atmospheric Sciences, Georgia Institute of Technology, Atlanta, Georgia, USA.
[8]School of Chemical and Biomolecular Engineering, Georgia Institute of Technology, Atlanta, Georgia, USA.
[9]Atmospheric Sciences Research Center, State University of New York at Albany, Albany, New York, USA.
[10]Atmospheric and Oceanic Sciences, University of Wisconsin–Madison, Madison, Wisconsin, USA.

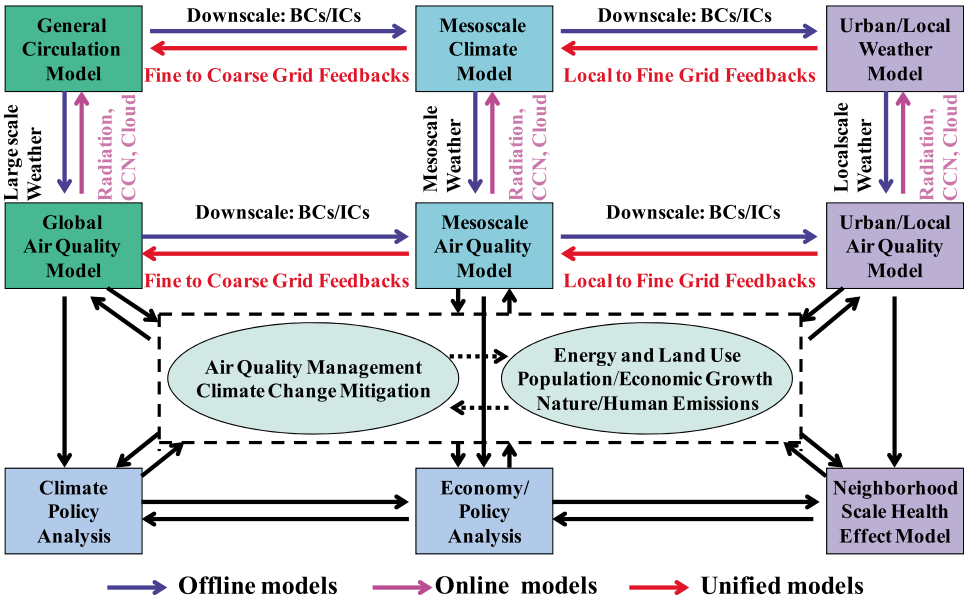


**Figure 1.** A generalized modeling system for linking climate, air quality, human health effect, and policy studies in offline- and online-coupled modes. The atmospheric processes in blue color can be treated in the offline-coupled systems, those in pink colors can only be treated in the online-coupled systems, and those in red color can only be treated in the unified global-through-urban systems.

climate variables (e.g., temperature, precipitation, and radiation) that affect emissions, chemical transformation, and transport processes of pollutants on global through urban scales, and (2) changes in vegetation and land cover that alter biogenic and anthropogenic emissions, dry deposition, and pollution export from the urban/regional environment to the global. The impact of global change cannot be fully understood in a simple cause-effect context, as global change and air quality are closely coupled through many meteorological, chemical, and radiative processes.

[3] Aerosols can affect climate directly through absorption and scattering and indirectly through the modification of cloud formation and evolution. Despite an increasing number of applications of online-coupled models [e.g., *Grell et al.*, 2005, 2011a; *Fast et al.*, 2006; *Zhang et al.*, 2010a, 2010b, 2012a; *Grell and Baklanov*, 2011; *Forkel et al.*, 2011; *Yu et al.*, 2011], the feedbacks from aerosols to boundary meteorology and radiation cannot typically be simulated in most current three-dimensional (3-D) models that do not couple meteorology and chemistry online. Those feedbacks, however, are important because they can have a profound impact on climate state and sensitivity to anthropogenic influences [e.g., *Jacobson*, 2002; *Chung and Seinfeld*, 2005; *H. Liao et al.*, 2009] and future climate changes may be affected by improved air quality [*Brasseur and Roeckner*, 2005].

[4] While climate responses to changes in gases and aerosols have been extensively studied in the past several decades [e.g., *Chuang et al.*, 1997; *Ghan et al.*, 2001; *Jacobson*, 2002; *Fiore et al.*, 2002; *Feichter et al.*, 2004; *Liao and Seinfeld*, 2005; *Chung and Seinfeld*, 2005; *Intergovernmental Panel on Climate Change* (*IPCC*), 2007; *H. Liao et al.*, 2009; *Chen et al.*, 2010], studies focused on the impact of global change on urban/regional air quality are limited. As shown in Figure 1, the impact of climate change on air quality is typically studied through a one-way approach using several offline-coupled models separately at different scales. These models typically include a general circulation model (GCM) that provides future meteorology/climate simulations; a global air quality model that is driven by GCM and provides boundary conditions to an urban/regional air quality model; a regional climate model that downscales the GCM to predict future regional climate change and a regional air quality model that predicts the impact of a future climate scenario on regional air quality. Some modeling systems also consist of an urban/local weather model that downscales the regional climate/meteorological model to predict future urban/local scale climate change, an urban air quality model that predicts the impact of future climate scenarios on urban/local scale air quality, and a neighborhood-scale human health/exposure model to predict the impact of urban/local air pollution on human health. These models at various scales require natural and anthropogenic emissions that are affected by population and economic growth, energy/fuel/technology use, and land use. The predicted changes in climate and air quality as well as human health impact on various scales can be used to guide the development of effective strategies for climate change mitigation and air quality management as well as relevant economy and climate policy analysis, all of which, as cyclical processes, will affect future population and economic growth, energy/fuel/technology use, and land use, and thus modify natural and anthropogenic emissions.

[5] While such an offline-coupled model system has been very useful for answering questions related to air quality [e.g., *Russell and Dennis*, 2000; *Seinfeld*, 2004; *Zhang*, 2008], it is subject to several limitations/uncertainties due to incomplete scientific understanding and computational restrictions. First, model transport and chemistry treatments

are inconsistent among all models in the system [e.g., *Sanderson et al.*, 2006; *Weaver et al.*, 2009] and thus introduce some uncertainties into model estimates. Second, global models use a spatial resolution that is too coarse to resolve atmospheric processes at urban/regional scales [e.g., *Johnson et al.*, 2001; *Mickley et al.*, 2004; *Langner et al.*, 2005; *Pye et al.*, 2009]. Interpolation errors in meteorological and chemical fields predicted from larger models at much coarser spatial and temporal resolutions occur when they are used to drive smaller scale models. Third, uncertainties exist in the downscaling techniques that may introduce errors [e.g., *Feser and von Storch*, 2008; *Liu et al.*, 2012]. Most importantly, the feedbacks among gases, aerosols, climate, meteorology, and radiation cannot be taken into account in many existing offline coupled models at both global and regional scales [e.g., *Giorgi and Shields*, 1999; *Prather et al.*, 2003; *Tagaris et al.*, 2007; *Pye et al.*, 2009; *Weaver et al.*, 2009; *K. J. Liao et al.*, 2009]. Such feedbacks can only be simulated in fully coupled climate/meteorology-chemistry online models, which have gained increasing attention [e.g., *Jacobson*, 2001a, 2001b; *Uno et al.*, 2003; *Grell et al.*, 2005; *Roeckner et al.*, 2006; *Neary et al.*, 2007]. In addition, the separation of global, mesoscale, and urban/local models does not permit the simulation of the feedbacks of phenomenal details at a smaller scale into the larger scales [e.g., *Hogrefe et al.*, 2004; *Tagaris et al.*, 2007; *Weaver et al.*, 2009], because such feedbacks can only be simulated in unified global through-urban models, as indicated in Figure 1. These model deficiencies in accurately representing detailed atmospheric processes and feedbacks have led to the largest uncertainties in current estimates of direct and indirect effects of aerosols on climate as well as the impact of climate on air quality [*IPCC*, 2007; *Zhang*, 2008]. While these past studies significantly advanced our understanding of various atmospheric processes and their interactions, they indicated a need to develop a framework that can resolve the aforementioned limitations to further understand scale separation, impacts of grid resolution, and biases associated with simplifications and mechanism inconsistencies.

[6] An ideal modeling system should be an online-coupled unified global through-urban modeling system [e.g., *Grell and Baklanov*, 2011] that enables the simulation of major feedbacks across scales with consistent model treatments in a single modeling framework. Such an integrated modeling system, of which few exist at the present time, represents a new scientific capability for the entire scientific community to study important problems that require a consideration of multiscale feedbacks, e.g., dust particles are lifted locally; they affect local and global circulations, which in turn affect their further lifting locally. It therefore provides a powerful tool to address two grand environmental challenges: climate change and air quality degradation, and the development of the optimal emission control strategies that lead to co-benefits for both issues. At present, very few 3-D climate and air quality models include detailed physical and chemical treatments, account for all major feedbacks, and can also be applicable for various spatial scales. For example, the Gas, Aerosol, Transport, Radiation, General Circulation, Mesoscale, and Ocean Model (GATOR-GCMOM) of *Jacobson* [2001a, 2001b, 2004] and *Jacobson et al.* [2007] represents gas, size- and composition-resolved aerosol, cloud, and meteorological processes from the global down to urban scales via nesting, allowing feedback from gases, aerosols, and clouds to meteorology and radiation on all scales in one model simulation. The Canadian global multiscale air quality model (GEM-AQ) of *Neary et al.* [2007] and *Kaminski et al.* [2008] is also a unified online-coupled model that accounts for many meteorology-chemistry feedback mechanisms and that can directly downscale to a regional domain at a finer horizontal grid resolution.

[7] In this study, an online-coupled unified model, i.e., the global-through-urban weather and forecasting model with chemistry (GU-WRF/Chem), is developed to simulate the interactions between climate/meteorology and air quality. The overall objectives are to develop a unified model system to address the above major model deficiencies and reduce uncertainties associated with current model estimates, validate this model system using available observations, and demonstrate the capability of the model system in simulating the interactions between global climate changes and urban/regional air quality through an initial application over progressively nested domains from the global to urban scales.

## 2. Model Development and Characteristics

[8] GU-WRF/Chem is based on the global WRF (GWRF) version 3.0 [*Richardson et al.*, 2005, 2007; *Skamarock et al.*, 2008] developed at California Institute of Technology (Caltech) in collaboration with U.S. NCAR and the mesoscale WRF/Chem version 3.0 initially developed by U.S. NOAA in collaboration with NCAR and multiple organizations and further developed by the lead author's group at North Carolina State University (NCSU). WRF is designed for the 1–10 km grid-scale research applications and operational forecasting. It is a non-hydrostatic model that fully conserves mass and includes several options of dynamic cores, physical parameterizations, and nesting [*Skamarock et al.*, 2008]. Since its first release in 2000, WRF has been developed rapidly and has evolved into several new versions for applications including a mesoscale WRF/Chem prediction system that fully couples meteorology and chemistry online [*Grell et al.*, 2005; *Fast et al.*, 2006; *Zhang et al.*, 2010a, 2012a], a regional climate WRF (RC-WRF) [*Done et al.*, 2005; *Liang et al.*, 2005a, 2005b], a hurricane WRF (H-WRF) [*Cangialosi et al.*, 2005], and GWRF. In addition, WRF and WRF-Chem have been applied at the large Eddy simulation scale [e.g., *H. Wang et al.*, 2009, 2010]. The default released mesoscale WRF/Chem v3.0 contains two hard-coded gas-phase chemical mechanisms, i.e., the second generation Regional Acid Deposition Model Mechanism (RADM2) [*Stockwell et al.*, 1990] and the Carbon-Bond Mechanism version Z (CBM-Z) [*Zaveri and Peters*, 1999] (which is a variant of the Carbon Bond Mechanism IV (CBM-IV) [*Gery et al.*, 1989]). The Kinetic PreProcessor (KPP) [*Salzmann*, 2008; *Grell et al.*, 2011b] is used in WRF/Chem as a chemical solver, which allows the implementation of additional gas-phase chemical mechanisms into WRF/Chem. At the time of the release of WRF/Chem v3.0, the equation files existed for RADM2 as well as several versions of the Regional Atmospheric Chemistry Mechanism (RACM) [*Stockwell et al.*, 1997]. The two aerosol modules available in WRF/Chem v3.0 are the Modal Aerosol Dynamics Model

for Europe (MADE) [*Ackermann et al.*, 1998] with the secondary organic aerosol (SOA) model (SORGAM) of *Schell et al.* [2001] (referred to as MADE/SORGAM), and the Model for Simulating Aerosol Interactions and Chemistry (MOSAIC) [*Zaveri et al.*, 2008]. An updated version of the CBM-IV, i.e., the 2005 version of CBM (CB05) of *Yarwood et al.* [2005] and *Sarwar et al.* [2008] and the Model of Aerosol Dynamics, Reaction, Ionization, and Dissolution (MADRID) of *Zhang et al.* [2004, 2010b] were incorporated into the mesoscale WRF/Chem v3.0 (referred to as WRF/Chem-MADRID) [*Zhang et al.*, 2010a, 2012a]. CB05 and its extension (e.g., CB05 with a chlorine (Cl) chemistry extension (CB05Cl)) were developed by the U.S. EPA and its contractor [*Sarwar et al.*, 2008]. CB05 has been used in the U.S. EPA's CMAQ as the default gas-phase mechanism. With the addition of over 60 reactions into CBM-IV, CB05 is more suitable for simulating biogenics, toxics, and species potentially important to particulate matter (PM) formation and acid deposition; it can also better simulate some conditions encountered in pristine areas, winter temperatures, and high altitude situations. WRF and WRF/Chem offer 1-way or 2-way nesting. At each coarse-grid time step, the fine grid boundary conditions (i.e., the lateral boundaries) are interpolated from the coarse grid simulation in both nesting modes, and the fine grid solution replaces the coarse grid solution for coarse grid points that lie inside the fine grid in the 2-way nesting modes [*Skamarock et al.*, 2008].

[9] In a parallel effort to the mesoscale WRF and WRF/Chem development at the U.S. NCAR and NOAA, GWRF was developed by Caltech/NCAR and has been applied to simulate the interannual variability of dust storms in the atmospheres of Mars and Titan [*Richardson et al.*, 2005, 2007] and global climate change [e.g., *Zhang et al.*, 2012b]. It uses non-conformal projections with a lat-long grid with a polar Fourier filter to avoid instabilities due to E-W distance between grid points becoming small near poles. GWRF was released in 2007 along with the mesoscale WRF v3.0. GWRF offers the same set of physical options for transport schemes and cloud microphysics as mesoscale WRF as described in *Skamarock et al.* [2008]. Despite large biases at high latitudes and over Arctic and Antarctic areas, it shows overall good performance in terms of the global zonal mean climatology [*Richardson et al.*, 2007] and major boundary layer meteorological variables [e.g., *Zhang et al.*, 2012b] as compared to observations from surface networks and satellites, which is also consistent with GCMs.

[10] The development of GU-WRF/Chem involves several steps. First, the mesoscale WRF/Chem-MADRID is globalized through linking it with GWRF. Second, several existing model treatments in WRF/Chem-MADRID are improved and new model treatments are incorporated to ensure an appropriateness of model treatments at all scales. These treatments include gas-phase chemistry, photolytic rate calculation, aerosol microphysics and chemistry, and aerosol-cloud interactions. Third, emissions of air pollutants from various emission inventories are assembled and regridded into the model grids and the improved/new model treatments are tested and further improved within GU-WRF/Chem. Fourth, sensitivity simulations are conducted to understand the impact of modified/new model treatments before their applications at various scales. These treatments are described below. The emissions assembly and regridding will be described as part of the model application in section 3. Sensitivity simulations using alternative model treatments will be described in section 4.

### 2.1. Gas-Phase Chemistry

[11] Major challenges in developing GU-WRF/Chem are to ensure the appropriateness of the chemical mechanism in simulating $O_3$, $PM_{2.5}$, their precursors, and mercury (Hg) in both troposphere and stratosphere and the interactions between aerosols and clouds. None of the existing mechanisms (i.e., RADM2, RACM, CBM-Z) in WRF/Chem v3.0 has such a capability. An appropriate gas-phase chemical mechanism is therefore needed in GU-WRF/Chem.

[12] In this study, a new chemical mechanism based on CB05 is developed for its global application (referred to as CB05 with global extension (CB05_GE)) [*Karamchandani et al.*, 2012] by adding Hg chemistry, the chemistry of the marine boundary layer, the chemistry of the upper troposphere and lower stratosphere, and Arctic chemistry. The CB05_GE mechanism is implemented into GU_WRF/Chem using the Kinetic PreProcessor (KPP) [*Salzmann*, 2008; *Grell et al.*, 2011b] and coupled with aerosol and aqueous-phase chemistry in GU-WRF/Chem. Compared with CB05, which includes 51 species and 156 reactions, CB05_GE contains 289 reactions among 118 species, with a total of 129 new reactions including 6 stratospheric reactions involving molecular oxygen ($O_2$), excited atomic oxygen ($O^1D$), methane ($CH_4$), nitrous oxide ($N_2O$), and carbon dioxide ($CO_2$) based on *Jacobson* [2005, 2008] and *Seinfeld and Pandis* [2006], 78 reactions for 25 halogen species (48 for 14 Cl and 30 for 11 Br species), 4 Hg reactions for elemental mercury (Hg(0)), divalent mercury Hg(II) (gas+PM), 14 heterogeneous reactions on aerosol/cloud and 10 reactions on polar stratospheric clouds (PSCs), and 17 oxidation reactions of volatile organic compounds (VOCs) (see *Karamchandani et al.* [2012, Tables 1–5] for these reactions). The heterogeneous reactions in CB05_GE contain 12 reactions on particle surfaces including the oxidation of $SO_2$ to sulfate on mineral aerosols based on *Dentener et al.* [1996]; 2 reactions on cloud droplets; and 10 reactions on Type I and Type II PSCs. The rate constants of the first-order reactions are first calculated as a function of the total surface area of particles, the reaction probability (also called the uptake coefficient) of the gas, and the thermal speed of the impinging gas following *Jacobson* [2005]. Second-order reaction rate constants are then determined for most of the reactions by dividing the first-order rate constants by the concentration of the adsorbed species, following the approach of *Kirner et al.* [2011]. Five species, i.e., water vapor ($H_2O$), $CH_4$, $O_2$, $CO_2$ and hydrogen ($H_2$), that are either not included or included as a constant in nearly all regional models, are treated as chemically reactive species, allowing the simulations of their emissions and/or chemical reactions. The production of $H_2O$ from the oxidation of $CH_4$ and other VOCs is explicitly treated to allow for feedback between the meteorological and chemistry components of WRF/Chem, while $CH_4$, $H_2$, and $CO_2$ are modeled species in GU-WRF/Chem with specified emission rates. $O_2$ is included to allow for its photolysis as a source of $O_3$ in the stratosphere. The reaction of $CO_2$ with $O^1D$ is added to account for its quenching based on *Jacobson* [2008]. In addition, many of the existing CB05 reactions were updated

to allow the explicit production of species such as $H_2O$ and $CO_2$. A more detailed description of the CB05_GE gas-phase chemical mechanism can be found in *Karamchandani et al.* [2012].

### 2.2. Aerosol Treatments and Radiation-Aerosol-Cloud-Precipitation Interactions

[13] Among the three aerosol modules in GU-WRF/Chem, MADRID is selected because it contains a secondary organic aerosol (SOA) module that is superior to that in MADE/SORGRAM and that is not included in MOSAIC (note that MOSAIC in WRF/Chem version 3.3 and newer contains a SOA module). MADRID is an aerosol module that treats all major aerosol chemical and microphysical processes including inorganic aerosol thermodynamic equilibrium, SOA formation, nucleation, gas/particle mass transfer, condensation, and coagulation. The inorganic aerosol thermodynamic equilibrium is based on ISORROPIA version 1.7 of *Nenes et al.* [1998]. As described in *Zhang et al.* [2010b], the SOA module simulates 25 SOA species formed by absorbing oxidation products of biogenic VOCs including isoprene and terpene, and anthropogenic VOCs including toluene, xylene, higher molecular alkanes, and polycyclic aromatic hydrocarbons. Terpene is split into sesquiterpene and five monoterpene families including surrogate species for $\alpha$-pinene and sabinene, surrogate species for $\beta$-pinene and $\Delta$3-carene, limonene, terpinene, and surrogate species for other monoterpenes. The binary homogeneous nucleation of sulfuric acid and water vapor is simulated based on the algorithm of *McMurry and Friedlander* [1979] that accounts for the competition between nucleation and condensation. Gas/particle mass transfer in MADRID is simulated with three algorithms: a bulk equilibrium approach that assumes full equilibrium between gas and particulate phases, a hybrid approach that treats mass transfer explicitly for coarse particles and assumes full equilibrium for fine particles, and a kinetic approach that solves the full aerosol dynamic equation. Full equilibrium is used as the default algorithm for GU-WRF/Chem model development and initial applications in this work. In the hybrid or kinetic approach, condensation and evaporation of condensable gas-phase species are explicitly simulated based on the analytical predictor of condensation of *Jacobson* [2005]. When the bulk equilibrium approach is used, condensation is implicitly treated by allocating the transferred mass to different size sections based on the condensational growth law as described in *Zhang et al.* [2004]. The growth of particles over sections with fixed size boundaries due to condensation and aqueous-phase chemistry is simulated using the moving-center scheme of *Jacobson* [2005]. The coagulation algorithm is based on the module of *Jacobson et al.* [1994].

[14] GU-WRF/Chem uses the same aerosol direct and indirect effect treatments as those for the mesoscale WRF/Chem, which were described in *Fast et al.* [2006] and *Chapman et al.* [2009]. A brief description is provided below. Aerosol radiative properties are simulated based on the Mie theory. Aerosol direct radiative forcing is calculated using the Goddard shortwave radiative transfer model of *Chou et al.* [1998]. The aerosol indirect effects are simulated through aerosol-cloud-radiation-precipitation interactions. Cloud Condensation Nuclei (CCN) spectrum is determined based on the Köhler theory as a function of aerosol number concentrations and updraft velocity following the aerosol activation/resuspension parameterization of *Abdul-Razzak and Ghan* [2002]. The subgrid updraft velocity is calculated from turbulence kinetic energy for all layers above surface and diagnosed from eddy diffusivity at the surface. The same parameterization was used to calculate updraft velocities on different nested domains in the GU-WRF/Chem simulations. Cloud droplet number concentrations (CDNC) are then predicted by accounting for their changes due to major cloud processes including droplet nucleation/aerosol activation, advection, collision/coalescence, collection by rain, ice, and snow, and freezing to form ice crystals following the parameterization of *Ghan et al.* [1997], which has been added to the existing Lin cloud microphysics scheme [*Lin et al.*, 1983; *Chen and Sun*, 2002] to allow the two-moment treatment of cloud water. The cloud-precipitation interactions are simulated by accounting for the dependence of autoconversion of cloud droplets to rain droplets on CDNC based on the parameterization of *Liu et al.* [2005]. The cloud-radiation interactions are simulated by linking simulated CDNC with the Goddard shortwave radiation scheme of *Chou et al.* [1998] and the Lin et al. microphysics scheme [*Skamarock et al.*, 2008]. Although the cloud treatments in the Lin et al. scheme in GU-WRF/Chem remain parameterized and they are based on the two-moment modal cloud size distribution, they are much more physically based, as compared to most models that use highly simplified cloud microphysics and diagnose CDNC.

[15] To ensure an adequate representation of aerosol processes and aerosol-cloud-precipitation interactions in GU-WRF/Chem, several aerosol-related treatments are improved in this work. CB05_GE is coupled with MADRID and MOSAIC to provide the gas-phase mechanism to produce precursors for secondary aerosols. It is also coupled with the Carnegie Mellon University (CMU) aqueous-phase chemical mechanism of *Fahey and Pandis* [2001], which allows additional aerosol formation in cloud and raindrops. The nucleation treatment in MADRID is improved through the incorporation of two nucleation parameterizations including the empirical power law (PL) of *Sihto et al.* [2006] and the ion-mediated nucleation (IMN) scheme of *Yu* [2010] (referred to as SI06 and YU10, respectively hereafter). SI06 uses the PL expression to calculate nucleation rates as a function of number concentrations of sulfuric acid ($H_2SO_4$) with the power order of 1 and a prefactor of $1.7 \times 10^{-6}$ that are derived based on the cluster-activation nucleation theory suggested by *Kulmala et al.* [2006] using observed nucleation rates from field campaigns in Europe. The prefactor $A$ is an empirical coefficient representing the actual physics and chemistry of the nucleation process. Its values may vary with location or season or time of sampling. SI06 is shown to be the most accurate nucleation parameterization among a number of binary, ternary, and empirical nucleation schemes tested to represent nucleation processes under urban conditions by *Zhang et al.* [2010a, 2010b]. YU10 is based on a kinetic model that explicitly solves the interactions among ions, neutral and charged clusters, vapor molecules, and pre-existing particles [e.g., *Yu and Turco*, 2000; *Yu*, 2006]. The ionization rates are affected by galactic cosmic rays (GCR) and some localized sources such as radioactive emanations, lighting, and nuclear waste [*Yu et al.*, 2010]. The simulation with YU10 uses a

lookup table for ionization rates, with GCR ionization based on the schemes of *Usoskin and Kovaltsov* [2006] and the contribution of radioactive materials from soil based on the profiles given in *Reiter* [1992]. In the lower troposphere, ionization rate (Q) is generally below 10 ion-pairs $cm^{-3}$ $s^{-1}$. In the upper troposphere, Q is in the range of 10–20 ion-pairs $cm^{-3}$ $s^{-1}$ at the low latitudes (30°S–30°N) and 20–40 ion-pairs $cm^{-3}$ $s^{-1}$ at the high latitudes. A zonally averaged annual mean Q values can be found in *Yu et al.* [2010]. Recent studies have shown that the physically-based IMN is supported by detailed field measurements (including the overcharging ratio of freshly nucleated particles) [*Yu and Turco*, 2011] and may provide an important source of new particles in the global atmosphere [*Yu et al.*, 2008; *Yu and Luo*, 2009]. By comparing global aerosol number concentration predictions based on six widely used nucleation schemes (two binary, two empirical, and two ion-mediated or ion-induced) with an extensive set of aerosol number concentration data derived from land, ship, and aircraft measurements, *Yu et al.* [2010] showed that only YU10 could reasonably account for both absolute values (within a factor of ~2) and spatial distributions of particle number concentrations in the entire troposphere. In this work, both SI06 and YU10 are therefore selected and implemented into GU-WRF/Chem as alternative nucleation parameterizations. Section 4 shows preliminary sensitivity test simulations using various nucleation parameterizations.

[16] Aerosol activation and scavenging are the direct microphysical links between aerosol and clouds and therefore critical to the estimation of aerosol indirect effects. The aerosol activation parameterization used in the publically released version of WRF/Chem is based on that of *Abdul-Razzak and Ghan* [2002] (ARG02). It uses an empirical prescribed value of geometric diameter and standard deviation and treats each section as a separate mode. In this study, the aerosol activation parameterization of *Fountoukis and Nenes* [2005] (FN05) has been incorporated into GU-WRF/Chem as an alternative aerosol activation parameterization. Similar to ARG02, FN05 has been coupled with the MADRID aerosol module and the CMU aqueous-phase chemical mechanism. Several differences exist between ARG02 and FN05. First, ARG02 calculates the maximum parcel supersaturation ($S_{max}$) explicitly by using a correlation derived from the regression of numerical parcel calculations. FN05 explicitly solves $S_{max}$ from the water balance equation using an adiabatic cloud parcel model with the "population splitting" technique that separates CCN with a size close to their critical diameter from those with other sizes. Second, FN05 includes an explicit treatment of mass transfer (i.e., kinetic) limitations in droplet growth, whereas ARG02 assumes instantaneous activation of CCN and equilibrium growth to its critical diameter when the parcel supersaturation equals the CCN's critical supersaturation without accounting for kinetic effects. Third, FN05 accounts for the size-dependence of the water vapor diffusivity coefficient and mass transfer coefficient for the growth of water droplets, which is neglected in ARG02. FN05 thus provides a more accurate treatment than many other parameterizations such as ARG02. Test results using the two different activation parameterizations are compared to examine their limitations and the sensitivity of aerosol indirect effects to these approaches in section 4.

### 2.3. Other Model Treatments

[17] To enable the aforementioned new/modified model treatments, several additional model treatments are revised. The photolytic reaction rates in GU-WRF/Chem are calculated using the Fast Tropospheric Ultraviolet-Visible (FTUV) model [*Tie et al.*, 2003]. CB05_GE contains 38 out of the 56 photolytic reactions included in the original FTUV and it treats 11 additional photolytic reactions that are not supported in the FTUV, including those of hypochlorous acid (HOCl), formyl chloride (FMCL), nitrohydrochloric acid ($ClNO_2$), hydrochloric acid (HCl, chlorine peroxide ($Cl_2O_2$), molecular bromine ($Br_2$), hypobromous acid (HOBr), nitryl bromide ($BrNO_2$), hypobromite (BrO), bromine chloride (BrCl), and hydrogen bromide (HBr). The photolysis data of these species in 17 wavelength bins are added in the FTUV based on *Sander et al.* [2006]. Since the default FTUV can only use the RADM2 gas-phase mechanism that is coupled with MADE/SORGAM, it includes only 21 photolytic reactions. To couple CB05_GE with the FTUV, the photolysis rates for additional 28 species are added in the interface between CB05_GE and FTUV to support CB05_GE and its coupling with MADRID. Since the FTUV does not calculate photolysis rates at the top model level in its default setting, it is modified in this work to provide photolysis rates for all model layers.

[18] Several changes are made in the online emission modules for mineral dust and biogenic VOCs to overcome some of their limitations, which are described in section 3.2.

## 3. Initial Application

### 3.1. Model Configuration and Evaluation Protocol

[19] GU-WRF/Chem simulations over five domains in 2001 January and July are conducted to evaluate the model performance. Table 1 summarizes the model configurations. Figure 2 shows the five domains including a global domain at 4° latitude × 5° longitude (D01), a Trans-Pacific domain at 1.0° × 1.25° (D02) covering Asia, the Pacific Ocean, and North America, two regional domains at 0.33° × 0.42° over the continental U.S. (D03) and East Asia (D04), and an urban domain at 0.08° × 0.10° over the eastern U.S. (D05). D01 provides a global assessment of the model capability and simulated meteorology and chemistry interactions and it also provides boundary conditions to nested domains. D02 allows an examination of the impact of intercontinental transport of air pollutants originating from Asia on air quality over the U.S. D03 and D04 are regional domains comparable to domains used for many past regional air quality simulations using WRF/Chem and other models such as CMAQ, thus permitting an intercomparison of model performance between GU-WRF/Chem and regional models. D05 allows an examination of the model capability on an urban scale. One-way nesting is used. The horizontal grid interpolation from the coarse grid simulation is performed every 20 min to generate time-dependent lateral boundary conditions for the nested domains.

[20] To separate the effects of PM from those of gases on model predictions, two sets of model simulations are conducted for each month. In the baseline simulations, all meteorological and chemical processes of gases and PM species are included. In the second set of simulations, all model treatments remain the same as the baseline simulation

**Table 1.** GU-WRF/Chem Configurations

| Attribute | Model Configuration |
|---|---|
| Simulation period | January 1–31 and July 1–31, 2001 |
| Domain | Global and nested regional/urban domains |
| Horizontal resolution | Global (D01): 4° × 5°, 45 (latitude) × 72 (longitude)<br>Trans-Pacific (D02): 1.0° × 1.25°, 44 × 192<br>North America (D03): 0.33° × 0.42°, 84 × 168<br>East Asia (D04): 99 × 177<br>Eastern U.S. (D05): 0.08° × 0.10°, 136 × 144 |
| Vertical resolution | 27 layers from 1000–50 mb, with 17 layers in PBL (<2.6 km) |
| Meteorological IC and BC | The National Centers for Environmental Predictions Final Analysis (NCEP-FNL) reanalysis data; re-initialization every 4 days |
| Shortwave radiation | Goddard shortwave radiation scheme [*Chou et al.*, 1998] |
| Longwave radiation | The rapid radiative transfer model (RRTM) [*Mlawer et al.*, 1997] |
| Land surface | Community National Centers for Environmental Prediction (NCEP), Oregon State University, Air Force, and Hydrologic Research Lab-NWS Land Surface Model (NOAH) [*Chen and Dudhia*, 2001; *Ek et al.*, 2003] |
| Surface layer | Monin-Obukhov [*Monin and Obukhov*, 1954; *Janjic*, 2002] |
| PBL | Yonsei University Scheme (YSU) [*Hong et al.*, 2006] |
| Cumulus | Kain-Fritsch (KF) II [*Kain and Fritsch*, 1990, 1993; *Kain*, 2004] |
| Microphysics | Purdue Lin [*Lin et al.*, 1983; *Chen and Sun*, 2002] |
| Aerosol activation | Abdul-Razzak and Ghan (A-R & G) [*Abdul-Razzak and Ghan*, 2002] |
| Gas-phase chemistry | CB05_GE [*Karamchandani et al.*, 2012] (Baseline) |
| Photolysis | F-TUV [*Tie et al.*, 2003] |
| Aerosol module | Model of Aerosol, Dynamics, Reaction, Ionization, and Dissolution (MADRID) [*Zhang et al.*, 2004, 2010b] (Baseline)<br>Model for Simulating Aerosol Interactions and Chemistry |
| Aqueous-phase chemistry | Carnegie Mellon University (CMU) mechanism of *Fahey and Pandis* [2001] |
| Chemical initial conditions | $O_3$, $N_2O$, and $CH_4$ from CCSM and the other moderately long-lived species are from GEOS-CHEM (GEOS-Chem v7-04-12 run0). The short-lived radicals are set to be clean conditions and aerosols are based on the default ICs from regional WRF/Chem. |
| Chemical boundary conditions | BCs for D02-D05 are from their respective parent domains |
| Anthropogenic/natural emissions | See Table 2 |

except that PM emissions and secondary PM formation processes are turned off, which essentially shuts off the feedbacks between meteorology and aerosols (except those caused by background concentrations of aerosols). Since both simulations use the same initial conditions for PM over the global domain and the same initial and boundary conditions for PM which represent relatively clean conditions on nested domains, the differences in model predictions between the two sets of simulations are caused by additional PM resulting from primary PM emissions and gas-to-particle conversions in a polluted environment; they provide an estimate of the aerosol feedbacks to shortwave radiation, PBL meteorology, and cloud formation. The aerosol feedbacks are analyzed using domain-wide monthly mean spatial

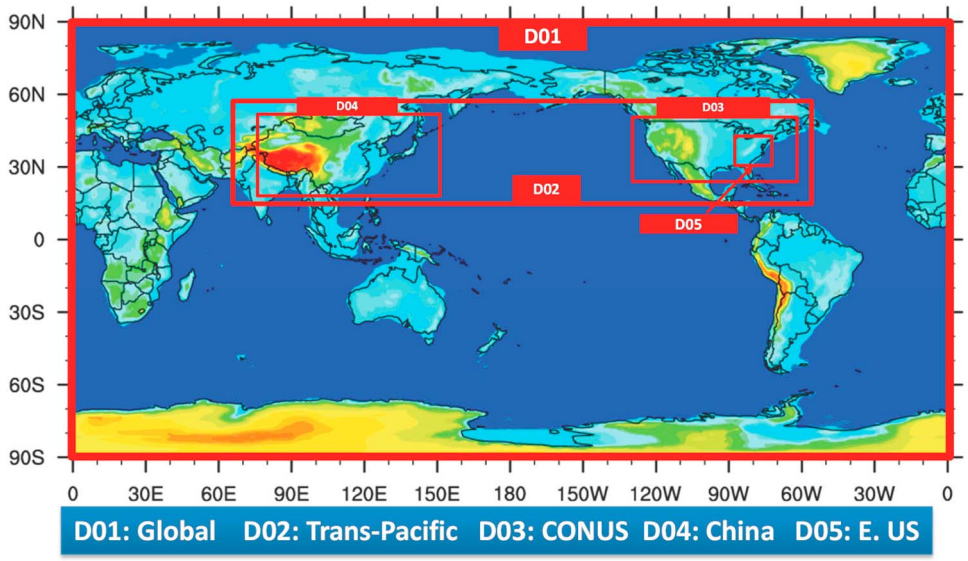


**Figure 2.** Simulation domains: Global (D01): 4° × 5°, 45 (latitude) × 72 (longitude), Trans-Pacific (D02): 1.0° × 1.25°, 44 × 192; CONUS (D03): 0.33° × 0.42°, 84 × 168, East Asia (D03): 99 × 177 (China), and Eastern U.S. (D04) 0.08° × 0.10°, 136 × 144.

distributions to minimize the chaotic nature of the relatively short model simulations. Region-specific vertical profiles are also examined to study the aerosol feedback signals in populated continents where the aerosol concentrations (and thus the feedback signals) are high. Sensitivity simulations using the FN05 droplet activation and the SI06 and YU10 nucleation parameterizations are also conducted.

### 3.2. Model Inputs

[21] While a number of global emission inventories exist, they may not contain all emitted species included in CB05_GE and none of them reflect the latest changes at urban/regional scales in rapidly growing regions such as Asia. In addition, the emissions of a species commonly included in different emission inventories may be different, so it is important to examine their fidelity before their usage for model applications. In this study, we therefore develop a global emission inventory that incorporates the latest development on regional scales and that represents the best publicly available emissions of gases, primary PM, and Hg from the literature and public web sites.

[22] Table 2 summarizes the emitted species and the sources of their emissions compiled for the global and nested regional domains. The emissions of ketone (KET), terpenes (TERP), sulfur dioxide ($SO_2$), nitric oxide (NO), carbon monoxide (CO), ammonia ($NH_3$), elemental carbon (EC), and organic matters (OM) are based on the Model for Ozone and Related chemical Tracers, version 4 (MOZART 4) at a grid resolution of $1^\circ \times 1^\circ$ and the emissions of $CH_4$, $N_2O$, $H_2$, acetaldehyde (ALD2), formaldehyde (FORM), ethane (ETHA), ethene (ETH), internal olefin (IOLE), olefin (OLE), isoprene (ISOP), methanol (MEOH), and ethanol (ETOH) are based on the Community Atmospheric Model version 4 (CAM4) at $\sim 2.8^\circ \times \sim 2.8^\circ$ (T42LR), both of which are provided by NCAR [*Emmons et al.*, 2010]. However, the total emissions of CO and nitrogen oxides ($NO_x$) from MOZART4 are much higher than those from the REanalysis of the TROpospheric chemical composition (RETRO) [*Schultz et al.*, 2007], the Global Fire Emissions Database (GFED) version 2 [*Randerson et al.*, 2007] (http://daac.ornl.gov/VEGETATION/guides/global_fire_emissions_v2.1.html), and the Intergovernmental Panel on Climate Change (IPCC) Special Report on Emission Scenarios (SRES) [*IPCC*, 2000] (http://www.grida.no/climate/ipcc/emission/); and they are therefore adjusted based on the total emissions of the IPCC and the monthly variations of the RETRO. The scaling factors used are 0.7 for CO emissions in both months and 0.7 for $NO_x$ emissions in July, 2001. The emissions of $CO_2$, cresol (CRES), higher carboxylic acid (AACD), formyl chloride (FMCL), hydrocarbon with three, five, and eight carbon atoms (HC3, HC5, HC8), xylene (XYL), toluene (TOL), and other inorganic primary $PM_{2.5}$ are taken from RETRO [*Schultz et al.*, 2007] at $0.5^\circ \times 0.5^\circ$. The emissions of methyl chloride ($CH_3Cl$), chlorine nitrite ($ClNO_2$) and hydrochloric acid (HCl) are from the Reactive Chlorine Emissions Inventory (RCEI) [*McCulloch et al.*, 1999; *Keene et al.*, 1999] (http://www.geiacenter.org/rcei/) at $1^\circ \times 1^\circ$ and the emissions of trichlorofluoromethane ($CFCl_3$ or CFC-11), dichlorodifluoromethane ($CF_2Cl_2$ or CFC-12) difluorochlorobromomethane ($CF_2ClBr$), and trifluorobromomethane ($CF_3Br$) are from the IPCC SRES at $1^\circ \times 1^\circ$. The emissions of Hg(0), Hg(II) (gas+PM), and particulate mercury (HgP) from anthropogenic, oceanic, volcanic and other natural sources as well as reemissions from land and ocean are based on *Seigneur et al.* [2001, 2004] and *Lohman et al.* [2008]. The emissions of paraffin (PARA) are calculated using the emissions of ALD2, IOLE, and OLE from CAM4, and those of HC3, HC5, HC8, and AACD from RETRO. The hourly emissions of $SO_2$, NO, $NO_2$, CO, $NH_3$, ALD2, FORM, ETHA, ETH, IOLE, OLE, ISOP, MEOH, ETOH, XYL, TOL, EC, OM, primary $SO_4^{2-}$, primary $NO_3^-$, and other inorganic primary $PM_{2.5}$ and $PM_{10-2.5}$ from regional emission inventories over North America (i.e., the U.S. 1999 National Emissions Inventory (NEI) version 3, http://www.epa.gov/ttn/chief/net/1999inventory.html) and East Asia [e.g., *Q. Zhang et al.*, 2009; *L.-T. Wang et al.*, 2010] are available at a grid resolution of $36 \times 36$ km$^2$ and used for D03 and D04, respectively. They are regridded to various grid resolutions for use over D05 and for replacement of their emissions over D01 and D02. The updated Asian emissions were developed using a technology-based, bottom-up methodology following the general approach of *Streets et al.* [2003] with more detailed activity/fuel categories based on a proper understanding of China's current combustion/process technologies [*Streets et al.*, 2006].

[23] Emissions of sea salt and mineral dust depend on meteorological conditions (horizontal wind speed and temperatures). They affect radiative transfer and thus induce dynamical feedbacks [e.g., *Ramanathan et al.*, 2001; *Jacobson*, 2002, 2005]. The changes in local winds will in turn affect further their lifting. Similarly, while temperature and photosynthetically active radiation (PAR) affect biogenic emissions, the effects of biogenic emissions can be fed back to temperature and PAR through their effects on solar and thermal-IR radiative transfer. Mineral dust emissions depend not only on meteorological variables but also additional parameters (e.g., soil moisture and land use), which in turn affect boundary layer structures and biogenic emissions. Those two-way feedbacks cannot be adequately represented using static emissions. Their emissions are therefore calculated online in GU-WRF/Chem to enable the feedbacks of meteorology on their emissions as well as their feedbacks on radiation and meteorology.

[24] The sea-salt emission module used in WRF/Chem v3.0 is based on the work of *Gong et al.* [1997] with an updated treatment for smaller sea-salt particles from *O'Dowd et al.* [1997]. A number of dust emission schemes have been developed in the past several decades [e.g., *Gillette and Passi*, 1988; *Marticorena and Bergametti*, 1995; *Draxler et al.*, 2001] to estimate dust emissions as a function of meteorological variables such as friction velocity, soil texture, surface roughness, and land-use characteristics. One of the dust emission modules available in WRF/Chem v3.0 is based on *Shaw* [2008] which calculates dust emissions as a function of surface wind stress, vegetation, and soil type and uses an upper bound of friction velocity of 100 cm s$^{-1}$ to eliminate unrealistically high dust emissions. However, it uses vegetation masks that are specific to Mexico applications (i.e., grass, shrub, and savanna), which are not appropriate for global applications. In this work, two land types (i.e., mixed shrub/grassland and barren or sparsely vegetated land) are added as possible sources of dust emissions. In

**Table 2.** Sources of Emission Inventories Used for Global and Regional Domains[a]

| Species | Sources | Spatial (Temporal) Resolution | Year | Available Domain |
|---|---|---|---|---|
| KET,[b] TERP | MOZART4 | 1° × 1° (monthly) | 2000 | Global |
| $CH_4$, $N_2O$, $H_2$ | CAM4 | ~2.8° × ~2.8° (T42LR) (monthly) | 2000 | Global |
| $CH_3Cl$, $ClNO_2$, HCl | RCEI | 1° × 1° (Annual) | 1990 | Global |
| CFC-11, CFC-12, $CF_2CLBR$, $CF_3BR$ | IPCC | 1° × 1° (Annual) | 2000 | Global |
| $CO_2$, CRES, AACD, FMCL, HC3, HC5, and HC8 | RETRO | 0.5° × 0.5° (monthly) | 2000 | Global |
| Hg(0), Hg(II) (gas+PM), HgP | AER, Inc. [*Lohman et al.*, 2008] | 1° × 1° (Annual) | 1998/1999 | Global |
| $SO_2$, NO, CO, EC, OM | MOZART4 | 1° × 1° (monthly), | 2000 | Global |
| | U.S. EPA NEI99v3 | 36 km × 36 km (hourly) | 2001 | North America |
| | 2006 Asian Emissions | 36 km × 36 km (hourly) | 2006 | East Asia |
| $NO_2$ | U.S. EPA NEI99v3 | 36 km × 36 km (hourly) | 2001 | North America |
| | 2006 Asian Emissions | 36 km × 36 km (hourly) | 2006 | East Asia |
| $NH_3$[c] | MOZART4/CAM4 | 1° × 1°/~2.8° × ~2.8° (monthly), | 2000 | Global |
| | U.S. EPA NEI99v3 | 36 km × 36 km (hourly) | 2001 | North America |
| | 2006 Asian Emissions | 36 km × 36 km (hourly) | 2006 | East Asia |
| ALD2, FORM, ETHA, ETH, IOLE, OLE, ISOP, MEOH, ETOH | CAM4 | 1° × 1° (T42LR) (monthly) | 2000 | Global |
| | U.S. EPA NEI99v3 | 36 km × 36 km (hourly) | 2001 | North America |
| | 2006 Asian Emissions | 36 km × 36 km (hourly) | 2006 | East Asia |
| XYL, TOL | RETRO | 0.5° × 0.5° (monthly), | 2000 | Global |
| | U.S. EPA NEI99v3 | 36 km × 36 km (hourly) | 2001 | North America |
| | 2006 Asian Emissions | 36 km × 36 km (hourly) | 2006 | East Asia |
| PARA[d] | CAM4 + RETRO | ~2.8° × ~2.8° for CAM4 (monthly) | 2000 | Global |
| | U.S. EPA NEI99v3 | 0.5° × 0.5° for RETRO (monthly) | 2000 | North America |
| | 2006 Asian Emissions | 36 km × 36 km (hourly) | 2001 | East Asia |
| | | 36 km × 36 km (hourly) | 2006 | |
| Other inorganic primary $PM_{2.5}$ | RETRO (Fire emissions) | 1° × 1° (monthly) | 2000 | Global |
| | U.S. EPA NEI99v3 | 36 km × 36 km (hourly) | 2001 | North America |
| | 2006 Asian Emissions | 36 km × 36 km (hourly) | 2006 | East Asia |
| Primary $SO_4^{2-}$, Primary $NO_3^-$, Other inorganic primary $PM_{10-2.5}$ | U.S. EPA NEI99v3 | 36 km × 36 km (hourly) | 2001 | North America |
| | 2006 Asian Emissions | 36 km × 36 km (hourly) | 2006 | East Asia |
| Biogenic VOCs | Modified Guenther based on *Guenther et al.* [1993] | Online module | N/A | Global |
| Mineral dust | Modified *Shaw* [2008] | Online module | N/A | Global |
| Sea salt | *Gong et al.* [1997] and *O'Dowd et al.* [1997] | Online module | N/A | Global |

[a]MOZART 4- the Model for Ozone and Related chemical Tracers, version 4; CAM4 - the Community Atmospheric Model version 4; RETRO - the REanalysis of the TROpospheric chemical composition; RCEI - Reactive Chlorine Emissions Inventory, http://www.geiacenter.org/rcei/; IPCC - the Intergovernmental Panel on Climate Change.

[b]KET = $CH_3COCH_3$ (MOZART4) + MEK (MOZART4-bb, anthro) + MEK (CAM4-biofuel).

[c]$NH_3$ = $NH_3$ (MOZART4: anthro, bb, biogenic, ocean) + $NH_3$ (CAM4: soil, animals).

[d]PARA is calculated as 0.4 × ALD2 (CAM4) +2.9 × HC3(RETRO) +4.8 × HC5 (RETRO) +7.9 × HC8 (RETRO) +2.8 × IOLE (CAM4) +1.8 × OLE (CAM4) + AACD (RETRO).

addition, a factor of 0.05 is used to scale down the predicted emissions to match the global emission estimate of *Zender et al.* [2003]. For emissions of biogenic species such as isoprene and monoterpenes, several schemes are developed to account for their dependences on temperature, PAR, and land use [e.g., *Guenther et al.*, 1993, 1994, 1995; *Pierce et al.*, 1998; *Levis et al.*, 2003; *Jacobson*, 2005]. The scheme used in this work is based on the modified Guenther biogenic emissions module [*Guenther et al.*, 1993, 1994; *Simpson et al.*, 1995]. This scheme was originally coupled with CBM-Z, RACM, and RADM which do not include the chemical reactions of terpenes. Therefore, the emissions of terpenes are mapped to isoprene, olefin, and xylene with constant distribution factors that are dependent on land use types for simulations using these gas-phase mechanisms. In this work, the emissions of terpenes generated from the Guenther scheme are directly mapped with those of terpenes treated in CB05_GE.

### 3.3. Evaluation Protocol

[25] Model performance is evaluated for both meteorological and chemical predictions from the global-through-urban domains using available surface and satellite observations as well as reanalysis data for January and July 2001. The satellite data sets include the Total Ozone Mapping Spectrometer/the Solar Backscatter UltraViolet (TOMS/SBUV), the Measurements Of Pollution In The Troposphere (MOPITT), the Global Ozone Monitoring Experiment (GOME), and the Moderate Resolution Imaging Spectroradiometer (MODIS). Global surface network data include the Baseline Surface Radiation Network (BSRN) and the National Climatic Data Center (NCDC). The reanalysis data include the National Oceanic and Atmospheric Administration Climate Diagnostics Center (NOAA/CDC), the Climate Prediction Center (CPC) Merged Analysis of Precipitation (CMAP), and the Global Precipitation Climatology Project (GPCP). Other observation-based data include the MODIS-derived cloud

droplet number concentration (CDNC) from *Bennartz* [2007]. Surface routine monitoring networks and special studies over North America include the Clean Air Status and Trends Network (CASTNET) (http://www.epa.gov/castnet/), the Interagency Monitoring of Protected Visual Environments (IMPROVE) (http://vista.cira.colostate.edu/improve/), the Aerometric Information Retrieval System (AIRS)-Air Quality System (AQS) (http://www.epa.gov/air/data/index.html), the Speciation Trends Network (STN), (http://nadp.sws.uiuc.edu/nadpoverview.asp), the Southeastern Aerosol Research and Characterization study (SEARCH) (http://www.atmospheric-research.com/studies/SEARCH/), and the National Atmospheric Deposition Program (NADP).

[26] The protocols for performance evaluation follow those used in *Zhang et al.* [2009a, 2009b, 2012a], including spatial distributions and statistics. Statistics include the mean bias (MB), the root mean squared error (RMSE), the normalized mean bias (NMB), the normalized mean error (NME), and correlations. The meteorological and radiative variables that are evaluated are downward shortwave radiation (SWDOWN), outgoing longwave radiation (OLR), cloud fraction (CF), aerosol optical depth (AOD), cloud optical thickness (COT), cloud water path (CWP), precipitating water vapor (PWV), cloud condensation nuclei (CCN), CDNC, temperature, water mixing ratio, and relative humidity at 2-m (T2, Q2, and RH2, respectively), wind speed at 10-m (WS10), wind direction at 10-m (WD10), and total daily precipitation (Precip). To evaluate all observations related to MODIS, the monthly mean predictions such as AODs and COTs are calculated as an average of column-integrated values during 1500–2000 UTC when the Terra satellite passes over the continental U.S., following *Roy et al.* [2007]. CWP includes cloud water from liquid, ice, rain, snow, and graupel [*Otkin and Greenwald*, 2008]. CDNC in warm cloud is calculated as an average value within the layer of 150∼800 m from the ground during cloudy periods. Chemical concentrations evaluated include 1-h and 8-h maximum average $O_3$, 24-h average $PM_{2.5}$ and its major components (i.e., sulfate ($SO_4^{2-}$), nitrate ($NO_3^-$), ammonium ($NH_4^+$), elemental carbon (EC), organic matter (OM), total carbon (TC), column concentrations of tropospheric CO and $NO_2$, and tropospheric $O_3$ residual (TOR)). The model performance is evaluated for all five domains and that over D02–D03 is compared with the performance of other modeling systems over the same or similar domains. These include the MM5/CMAQ simulation over D02 by *K. Wang et al.* [2009] and the mesoscale WRF/Chem-CBM-Z-MOSAIC simulation by *Zhang et al.* [2010a], the mesoscale WRF/Chem-CB05-MADRID simulation by *Zhang et al.* [2012a], and the MM5/CMAQ simulation by *Zhang et al.* [2009a] over D03.

### 3.4. Model Evaluation

[27] Table 3 summarizes model performance statistics for meteorological and radiative predictions of GU-WRF/Chem over the five domains and their comparison with regional modeling systems applied previously over the same or similar domains. Compared with observations from BSRN, the predicted LWDOWN shows very good agreement with NMBs within 3.2% and NMEs within 6.1%, but the model moderately overpredicts SWDOWN with NMBs of 12.6–27.0% and NMEs of 12.7–27.0% in both months over D01–D03 (note that the statistics over D04–D05 are not calculated because of very small numbers of observational and simulation data pairs). The model moderately overpredicts SWDOWN against data from CASTNET and SEARCH over all domains with MBs of 41.3–62.1 W $m^{-2}$, NMBs of 34–52%, and NMEs of 45.2–55.7% in January and 60.1–83.1 W $m^{-2}$, 19.1–32.1%, and 32.7–45.8%, respectively, in July. The overpredicted SWDOWN can be partly attributed to the fact that the effect of cumulus clouds on radiation is not accounted for in this version of WRF/Chem since the Kain-Fritsch II cumulus scheme is not coupled with radiation. The model performs relatively well for OLR (with MBs < 13 W $m^{-2}$, NMBs < 6.3%, and NMEs < 7.1%) and PWV(with MBs within 0.15 $m^{-2}$, NMBs within 18.7%, and NMEs < 15.0%) in both months. Moderate underpredictions occur in CF (with MBs of −28% to −10.8%, NMBs of −39.4% to −16.1%, and NMEs of 25.4–39.4%) in January and −18.3% to −7.2%, −32.6% to −10.3%, and 25.4–37.1%) in July, and significant underpredictions occur in CWP (with NMBs of −86.2% to −74.5% and NMEs of 76.4–86.2%) and COT (with NMBs of −85.1% to −70.3% and NMEs of 73.5–85.1%) in both months. In addition to the underpredicted CWP, the COT calculation only accounts for contributions from water and ice in WRF/Chem, and both factors are responsible for the underpredictions in COTs. The underpredictions in CWP are mainly caused by limitations in current cloud microphysical parameterizations (e.g., the contribution of convective clouds to CWP is not accurately simulated) [*Zhang et al.*, 2012a]. The moderate/large underpredictions in CF, CWP, and COT are mainly responsible for overpredictions in SWDOWN. Column CCN over the oceans is underpredicted with NMB of −18.5% and NME of 56.3% in January and NMB of −8.7% and NME of 43.6% in July in D01 but overpredicted moderately to significantly with NMBs of 20–128.2% and NMEs of 54.9–72.1% over D02–D05 (except for D04 in January, over which the NMB is −1%). CNDC is largely underpredicted with NMBs of −72.1% to −41.2% and NMEs of 56.2–128.2% over all domains in both months, which is closely related to the underpredictions in CF, CWP, and COT. AOD is overpredicted significantly over all domains in July and over D01 in January but slightly underpredicted over D03–D05 in January, which are associated with model biases in PM predictions at surface and aloft (e.g., large overpredictions of surface $PM_{2.5}$ occur at the IMPROVE sites). Comparisons with the CMAP data show that Precip, on other hands, is moderately overpredicted in January over all domains and in July over D01, D02, and D04 but largely overpredicted in July over D03 and D05. When comparing with the GPCP daily precipitation data, overpredictions also dominate in D01 and D03–D05 in July and in D04 in January. Comparing with the NCDC daily precipitation, moderate overpredictions over D01, D02, and D04 (except for D01 in Jan.) and significant overpredictions over D03 and D05. Such overpredictions indicate too frequent rains predicted by the Kain-Fritsch II cumulus parameterization, a major limitation for many cumulus parameterizations that use the rain-bearing systems to establish mean precipitation climatology [*Randall et al.*, 2007]. In addition, the Lin et al. cloud microphysics scheme has a tendency to overpredict Precip. Comparing with observed T2 data from NCDC, the model gives large warm biases in terms of NMBs in Jan. due to the occurrence of the near zero observed T2.

**Table 3.** 2001 January and July Monthly Mean Normalized Mean Bias (NMB) in % of Meteorological/Radiative Variables

| | | | Trans Pacific (D02) | | CONUS (D03)[b] | | | | | |
|---|---|---|---|---|---|---|---|---|---|---|
| Variable[a] | Data Set | Global (D01), GU-WRF/Chem | GU-WRF/Chem | MM5/CMAQ[b] | GU-WRF/Chem | MM5/CMAQ[c] | Meso-WRF/Chem[d] | Meso-WRF/ Chem-MADRID[e] | East Asia (D04), GU-WRF/Chem | E. U.S. (D05), MM5/CMAQ |
| LWDOWN (W $m^{-2}$) | BSRN | 0.4/−0.8[f] | −3.0/−3.2 | | −2.2/−3.1 | | | | – | – |
| OLR (W $m^{-2}$) | NOAA-CDC | 6.0/2.3 | 4.0/1.1 | – | 4.7/2.1 | – | – | –/−2.6 | 4.8/1.6 | 6.3/1.8 |
| SWDOWN (W $m^{-2}$) | BSRN | 16.1/13.7 | 25.5/12.6 | | 27.0/15.9 | | | | – | – |
| | CASTNET | 34/26.4 | 37.2/21.0 | – | 41.4/19.1 | – | – | –/22.7 | | 52/21.5 |
| | SEARCH | 42.3/33.2 | 38.9/32.1 | – | 35.1/31.1 | – | – | –/17.3 | – | 48.3/19.7 |
| Cloud fraction | MODIS | −16.1/−10.3 | −21.6/−18.5 | – | −30.2/−32.6 | – | – | –/−5.6 | −35.5/−18.7 | −39.4/−26.8 |
| Column CCN (ocean) at S = 0.5% ($cm^{-2}$) | MODIS | −18.5/−8.7 | 38.7/20.1 | – | 91.1/58.0 | – | – | –/178.7 | −1.1/55.8 | 128.2/82.3 |
| CDNC ($cm^{-3}$) | BE09[g] | −47.1/−41.2 | −45.9/−53.0 | – | −66.5/−68.8 | – | – | –/−47.4 | −52.0/−31.3 | −72.1/−60.7 |
| COT | MODIS | −77.2/−75.5 | −74.6/−71.5 | – | −81.9/−84.6 | – | – | –/−76.4 | −73.4/−70.3 | −85.1/−80.6 |
| CWP (g $m^{-2}$) | MODIS | −80.2/−77.9 | −78.1/−75.1 | – | −84.2/−85.6 | – | – | –/−67.4 | −77.3/−74.5 | −86.2/−81.6 |
| PWV (cm) | MODIS | −2.5/−5.7 | −1.8/−9.2 | – | 1.8/−12.3 | – | – | –/−11.5 | −4.4/−8.6 | 18.7/−8.4 |
| AOD | MODIS | 69.7/97.9 | 3.1/51.9 | −37.9/−47.5 | −12.2/56.5 | −32.0/−34.8 | −64.6/3.7 | –/5.0 | −16.3/76.3 | −15.6/96.3 |
| Precip (mm $day^{-1}$) | GPCP | −4.5/2.3 | 5.1/−3.6 | | −13.7/43.3 | | | | 62.6/5.4 | −42.2/74.8 |
| | CMAP | 11.5/5.7 | 15.9/14.5 | – | 12.4/44.8 | –/41 | –/35 | –/55.6 | 21.5/23.5 | 13.0/63.1 |
| | NCDC | −9.4/9.3 | 18.8/22.0 | | 64.4/98.2 | | | | 15.1/13.0 | 92.3/115.0 |
| | NADP | – | – | −35.9/−41.0 | – | – | 21.2/32.3 | –/54.0 | – | – |
| T2 (°C) | NCDC | 37.3/0.5 | 737.2/−2.8 | | 280.4/−3.2 | | | | 71.0/−2.5 | 60.6/−0.7 |
| | CASTNET | −7.4/3.8 | −6.1/3.8 | −54.1/−0.9 | −4.2/1.9 | – | −13.7/0.3 | –/2.9 | – | −2.2/3.8 |
| | STN | −7.7/−5.0 | 0.4/−4.7 | −54.3/−10.0 | 6.4/−3.9 | – | 0.8/−6.1 | –/−3.8 | – | 1.5/−1.0 |
| | SEARCH | 7.2/−2.4 | 0.7/−1.9 | −38.1/−9.9 | 6.1/0.0 | – | −3.1/1.5 | –/0.6 | – | 13.2/5.7 |
| RH2 (%) | CASTNET | 12.1/3.1 | 8.4/−1.1 | 27.5/0.0 | 5.3/−1.3 | – | 9.5/−0.5 | –/−5.2 | – | 5.5/−2.3 |
| | SEARCH | 1.0/−6.3 | −1.8/−8.9 | 18.0/7.2 | −5.0/−12.9 | – | −0.2/−10.5 | –/−14.9 | – | −5.5/−13.1 |
| Q2 | NCDC | 11.1/4.8 | 15.9/4.2 | | 8.5/−0.9 | | | | 14.0/3.7 | 8.5/2.4 |
| WS10 (m $s^{-1}$) | NCDC | 58.9/30.3 | 60.2/25.6 | | 32.7/7.6 | | | | 92.7/58.3 | 21.3/1.5 |
| | CASTNET | 78.9/60.1 | 76.7/69.8 | 13.7/19.5 | 82.1/77.7 | – | 89.6/78.1 | –/98.4 | – | 71/96.7 |
| | SEARCH | 49.2/24.8 | 68.4/46.3 | 27.4/−0.2 | 63.8/51.8 | – | 40.5/33.1 | –/50.4 | – | 32.8/69.0 |
| WD10 (°) | CASTNET | 12.3/11.2 | 8.7/8.4 | −6.9/−4.7 | 8.8/6.3 | – | 8.9/0.9 | –/5.9 | – | 8.7/2.9 |
| | SEARCH | −7.5/5.4 | −3.2/2.2 | 6.0/−13.2 | −0.5/4.5 | – | −1.3/2.9 | –/5.4 | – | 1.3/8.1 |

[a]T2, temperature at 2-m; Q2, water mixing ratio at 2-m; RH2, relative humidity at 2-m; WS10, wind speed at 10-m; WD10, wind direction at 10-m; Precip, total daily precipitation; SWDOWN, downward shortwave; OLR, outogoing longwave radiation; CF, cloud fraction; CCN, cloud condensation nuclei; CDNC, cloud droplet number concentration; COT, cloud optional depth; LWP, cloud liquid water path; PWV, precipitable water vapor; dash, no observational data are available.

[b]All statistics are taken from *K. Wang et al.* [2009].

[c]All statistics are taken from *Zhang et al.* [2009a].

[d]All statistics are taken from *Zhang et al.* [2010a] using WRF/Chem version 2.2.

[e]All statistics are taken from *Zhang et al.* [2012a] using WRF/Chem-CB05-MADRID version 3.0.

[f]Read 0.4/−0.8 as NMB 0.4% for Jan 2001 and NMB −0.8% for July 2001.

[g]The observed CDNC values are taken from *Bennartz* [2007] (BE09).

The NMBs in July are within ±3%. Small cold biases occur in T2 at the CASTNET sites (mostly rural/remote sites) in January (with MBs of −0.4 to −0.1°C, NMBs of −13.7% to −2.2%, and NMEs of 45.5–52.3%) and small warm biases (with MBs of 0.4–0.8°C, NMBs of 1.9–3.8%, and NMEs of 7.6–10.3%) occur in July. For urban and rural sites, small cold biases occur at the STN sites in all domains and at the SEARCH sites in D01–D02 in July and small warm biases occur in January except at the STN sites over D01. For example, at the STN sites, MBs and NMBs are −1.3 to −0.2°C and −7.7% to −1%, respectively, in July over all domains and in January over D01; and MBs and NMBs are 0.03–0.5°C and 0.4–6.4%, respectively, in January over D02, D03, and D05. The model performs well for Q2 against NCDC data, with NMBs less than 16% in Jan. and within ±5% in Jul. The model also performs well for RH2, with NMBs within 12% and NMEs of 11.0–17.3% at the CASTNET sites and NMBs within 13.1% and NMEs of 11.0–17.3% at the SEARCH sites. While the simulated WD10 slightly deviates from the observations (within 25° or by <13.2%), large overpredictions occur in WS10 in both months, with NMBs of 60.1–96.7% at the CASTNET sites and 24.8–69.0% at the SEARCH sites. Using higher resolutions in nested domains can generally improve the model performance of the predictions of T2 and WD10 at most sites in both months, and RH2 in January against the CASTNET sites, and SWDOWN in July. The model performance at finer grid resolutions over smaller domains is degraded for some variables such as WS10, Precip, CF, CCN, CDNC, COT, and CWP.

[28] Compared with regional model simulations at a horizontal grid resolution of 108 × 108 $km^2$ using MM5/CMAQ over D02 [*K. Wang et al.*, 2009], GU-WRF/Chem performs much better for T2, RH2, and AOD in January, slightly better or comparably for T2, RH2, and AOD in July and WD10 in both months, and much worse for WS10 in both months. Compared with regional model simulations at a horizontal grid resolution of 36 × 36 $km^2$ using MM5/CMAQ over D03 [*Zhang et al.*, 2009a], the predictions of AOD from GU-WRF/Chem agree much better in January but much worse in July, and those of Precip against the CMAP data from GU-WRF/Chem are comparable. Compared with regional model simulations at a horizontal grid resolution of 36 × 36 $km^2$ using mesoscale WRF/Chem-CBMZ-MOSAIC (version 2.2) over D03 [*Zhang et al.*, 2010a], GU-WRF/Chem gives overall comparable performance for all variables, except for better AOD in January, and worse Precip and AOD in July and WS10 at the SEARCH sites in both months. Comparing with regional model simulations at a horizontal grid resolution of 36 × 36 $km^2$ using the mesoscale WRF/Chem-CB05-MADRID (version 3.0) over D03 in July, GU-WRF/Chem performs either better or comparably for all variables except for SWDOWN at the SEARCH sites, and domain-wide CF, COT, CDNC, CWP, and AOD.

[29] As shown in Figure 3, the spatial distribution of observed LWDOWN is well reproduced in both months. That of observed SWDOWN is overall well reproduced except for some overpredictions at a few sites in Australia and in the southern Pacific Ocean in January and in the U.S., Australia, and the southern hemisphere in July. D04 contains only one BSRN site and D05 contains only three sites. The predicted LWDOWN and SWDOWN at these sites are well reproduced (see Figure 3b for comparison over D05). Figure 4 shows the simulated and observed spatial distributions of several variables in both months. In both months, simulated OLR shows an overall good agreement with observations in terms of magnitudes and spatial distribution (despite some overpredictions over northern Africa, southern North America, northern South America) except for the areas between 45 and 90°N in Northern Hemisphere where the model significantly underpredicts OLR and also fails to reproduce its spatial distributions. CCN near most coastal lines is well predicted, although overpredictions occur in remote marine areas in Northern Hemisphere in both months and underpredictions occur in the southern oceans between 45 and 90°S in January. CNDC is overall well predicted in most regions near the coastlines but significantly underpredicted over land and moderately underpredicted over oceanic areas in both months. Simulated precipitation captures major patterns and magnitude of observations, although large overpredictions occur over the tropics.

[30] Table 4 summarizes model performance statistics for chemical predictions of GU-WRF/Chem over the five domains and their comparison with regional model systems. GU-WRF/Chem well predicts CO with NMBs within 11.5% and NMEs of 46.6–59.7%, but significantly underpredicts $SO_2$, $NO_x$, and $HNO_3$ at the SEARCH sites over all domains with NMBs of −66.1% to −8.2%, −98.0% to −8.4%, and −44.3% to −14.7% and NMEs of 65.5–86.3%, 66.1–98.3%, and 70.1–89.5%, respectively. Despite overpredictions in SWDOWN, maximum 1-h and 8-h average $O_3$ mixing ratios are slightly underpredicted at the AIRS-AQS sites except for D05 in July (NMBs of −17.8% to −10.2% and NMEs of 19.6–35.7%) and SEARCH (NMBs of −14.3% to −1.1% and NMEs of 17.2–26.0%) sites except for D05 in January but slightly to moderately underpredicted at the CASTNET sites in both months (NMBs of −31.4% to −3.8% and NMEs of 19.4–35.5%), implying possible underestimates in the emissions of precursors such as $NO_x$. This is supported by the large underpredictions in $NO_x$ mixing ratios. 24-h average concentrations of $PM_{2.5}$ are moderately to-significantly overpredicted at the IMPROVE sites in both months (NMBs of 6.0–138.3% and NMEs of 37.4–149.3%) and slightly overpredicted at the STN sites in July (NMBs of 5.8–13.8%) and the SEARCH sites in all domains in July and D03 and D05 in January (NMBs of 0.8–10.3%). They are moderately underpredicted at the STN sites (NMBs of −36.7% to −7.1%) and at the SEARCH sites (NMBs of −8.6% to −0.9%) over D01–D02 in January. The $PM_{10}$ number concentrations in the PBL are overpredicted over all domains, which is likely associated with possible overpredictions of $PM_{10}$ mass concentrations and other model uncertainties in the simulated precursor gas concentrations, nucleation rates, growth rates of nucleated particles, and other processes influencing particle number concentrations. In addition to uncertainties in the emissions of primary $PM_{2.5}$ (e.g., EC and OM) and secondary $PM_{2.5}$ precursors (e.g., $NH_3$, $NO_x$, $SO_2$, and VOCs), other possible reasons for overpredictions in $PM_{2.5}$ and $PM_{10}$ include overpredictions in SWDOWN in both months, underpredictions in T2 and overpredictions in RH2 at the CASTNET sites in January, underpredictions in T2 at the STN sites in July. The main reason for underpredictions in $PM_{2.5}$ in January is the overpredictions in Precip. We note small-to-large underpredictions

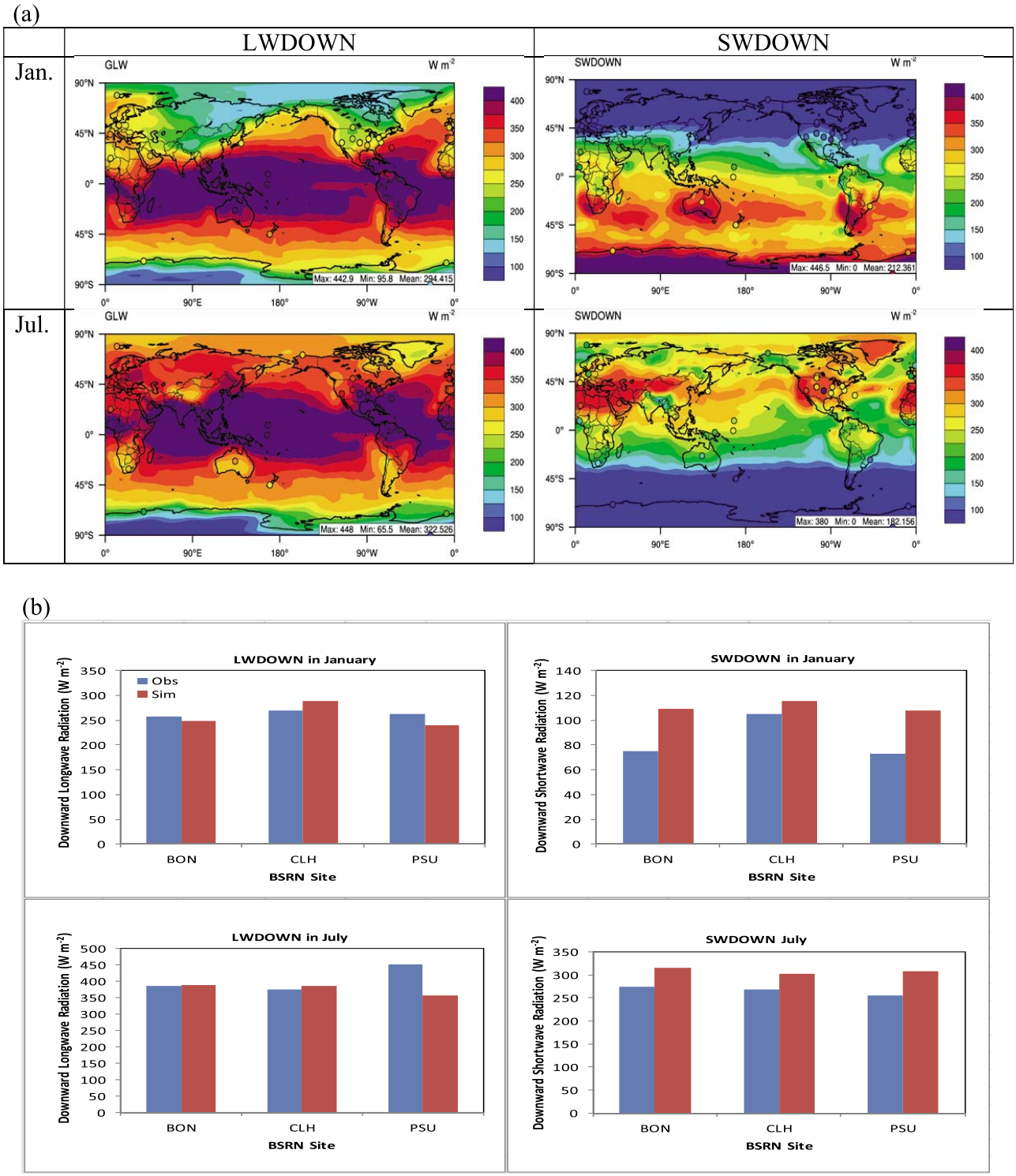


**Figure 3.** Simulated and observed monthly mean LWDOWN and SWDOWN (a) over D01 and (b) at three sites: Bondville, IL (BON), Chesapeake Light, North Atlantic Ocean (CHL), and Rock Springs, Pennsylvania (PSU) in D05. The observations are taken from the Baseline Surface Radiation Network (BSRN) in January and July 2001 and they are denoted by cycle symbols in Figure 3a and blue bars in Figure 3b.

in the concentrations of $NH_4^+$ and $SO_4^{2-}$ (except for $NH_4^+$ concentrations at the IMPROVE sites over D01 and D02 in both months and at the SEARCH site over D05 in January) imply possible underpredictions in the emissions of $NH_3$ and $SO_2$ and the oxidation of $SO_2$, as well as overpredictions in the wet scavenging of chemical species due to overpredictions in Precip. Nitrate concentrations are significantly overpredicted at the CASTNET, IMPROVE, and SEARCH sites

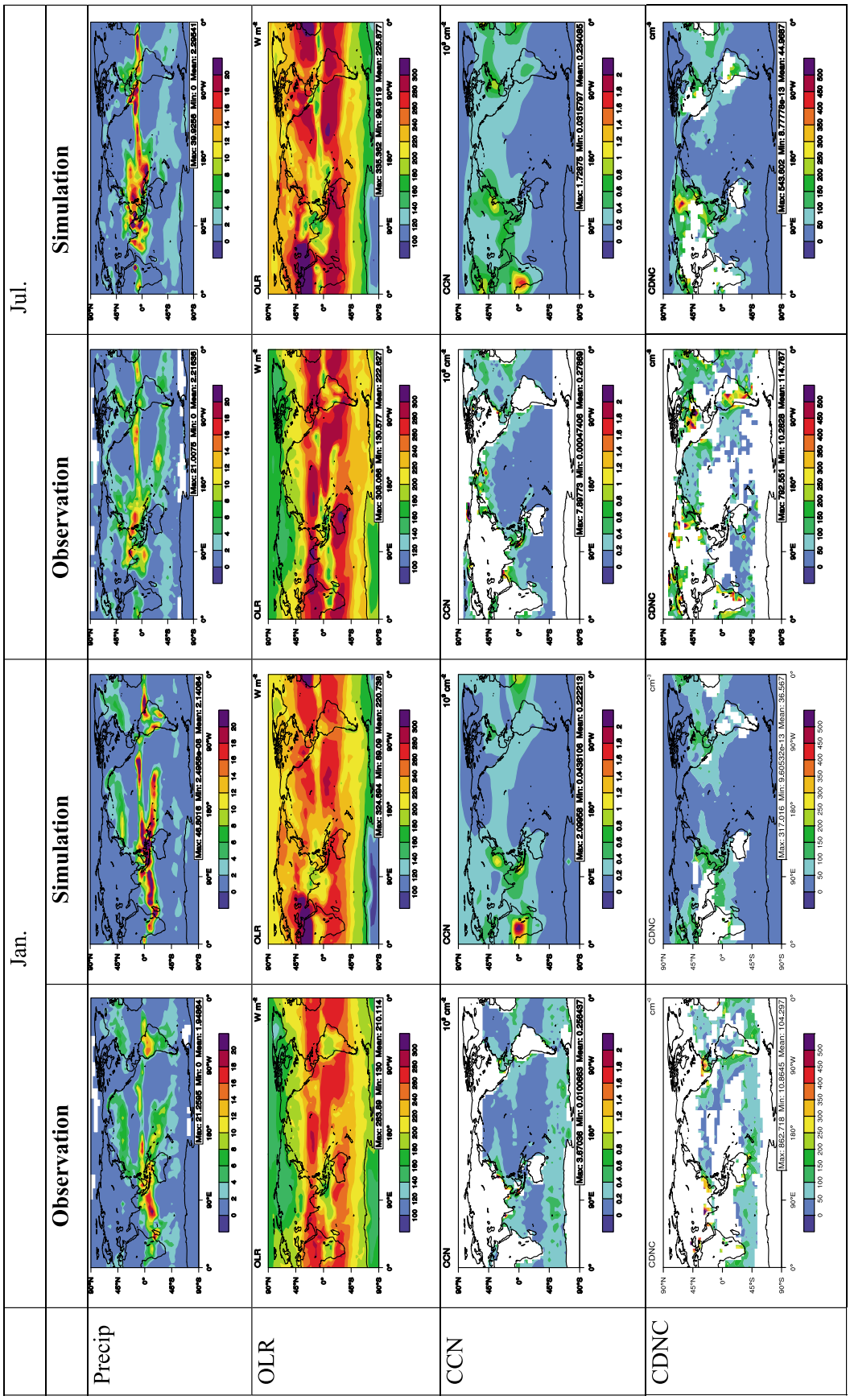


**Figure 4.** Observed and simulated variables. The observed precipitation, OLR, CCN, and CDNC are taken from CMAP, NOAA-CDC, MODIS, and *Bennartz* [2007], respectively.

**Table 4.** 2001 January and July Monthly Mean Normalized Mean Bias (NMB) in % of Chemical Variables

| Variable | Data Set | Global (D01), GU-WRF/Chem | Trans Pacific (D02), GU-WRF/Chem | | CONUS (D03) | | | | East Asia (D04), GU-WRF/Chem | E. U.S. (D05), GU-WRF/Chem |
|---|---|---|---|---|---|---|---|---|---|---|
| | | | GU-WRF/Chem | MM5/CMAQ[a] | GU-WRF/Chem | MM5/CMAQ[b] | Meso-WRF/Chem[c] | Meso WRF/Chem-MADRID[d] | | |
| CO | SEARCH | −10.8/−4.3 | −3.8/1.5 | – | 8.8/11.5 | – | – | –/0.1 | – | 7.6/−2.0 |
| $SO_2$ | SEARCH | −66.1/−45.9 | −62.2/−37.4 | – | −52.4/−15.8 | – | – | –/64.4 | – | −47.1/−8.2 |
| NO | SEARCH | −95.0/−98.0 | −93.0/−96.8 | – | −87.3/−94.0 | – | – | –/−91.2 | – | −88.3/−95.3 |
| $NO_2$ | SEARCH | −76.7/−76.9 | −64.5/−59.9 | – | −45.3/−17.0 | – | – | –/−12.7 | – | −45.9/−8.4 |
| $HNO_3$ | SEARCH | −23.1/−44.3 | −14.7/−36.2 | – | −17.2/−22.5 | – | – | –/87.6 | – | −49/−49.5 |
| Max 1-h $O_3$ | CASTNET | −31.4/−16.8 | −29.3/−17.5 | −22.6/−12.1 | −26.2/−16.3 | −21.4/−13.3 | −22.6/9.7 | –/2.8 | – | −27.1/−3.8 |
| | AIRS-AQS | −13.8/−17.8 | −10.2/−16.7 | 3.2/−0.7 | −10.6/−10.5 | −6.2/−10.5 | −13.2/12.8 | –/4.3 | – | −13.8/1.1 |
| | SEARCH | −1.1/−14.3 | −7.0/−14.1 | −12.2/4.3 | −10.8/−7.7 | 3.3/10.2[e] | −10.8/21.8 | –/23.9 | – | 2.8/−12.8 |
| Max 8-h $O_3$ | CASTNET | −30.0/−10.3 | −28.0/−11.8 | −16.1/−4.2 | −24.9/−12.4 | −14.8/−5.5 | −22.5/14.5 | –/7.0 | – | −25.4/0.2 |
| | AIRS-AQS | −5.8/−8.9 | −3.6/−8.2 | 11.3/6.2 | −4.5/−4.3 | 2.6/−0.4 | −10.8/18.1 | –/9.8 | – | −10.6/5.8 |
| | SEARCH | 5.8/−3.5 | −1.9/−3.8 | −5.7/19.0 | −6.8/0.4 | 6.4/15.9[e] | −9.8/30.5 | –/33.3 | – | 9.5/−4.9 |
| 24-h avg. $PM_{2.5}$ | IMPROVE | 138.3/44.6 | 70.8/27.7 | 155.8/27.0 | 45.5/18.2 | 29.7/−9.1[e] | 32.2/8.5 | –/5.5 | – | 38.3/6.0 |
| | STN | −29.1/13.8 | −36.7/7.4 | 22.3/21.7 | −27.6/7.9 | 1.3/−1.4[e] | −6.7/21.5 | –/−2.2 | – | −7.1/5.8 |
| | SEARCH | −0.9/8.7 | −8.6/10.3 | 23.5/32.9 | 0.8/8.5 | 24.9/41.0[e] | 23.7/33.1 | –/7.9 | – | 4.5/2.2 |
| $PM_{10}$ number[f] | YL09 | 85.2 | 110.8 | – | 99.9 | – | – | – | – | – |
| 24-h avg. $NH_4^+$ | CASTNET | −28.3/−22.5 | −34.8/−14.8 | 17.8/22.0 | −39.1/−25.0 | 1.8/11.6 | −64.4/84.4 | –/−13.0 | – | −31.4/−20.6 |
| | IMPROVE | 44.8/26.5 | 5.0/31.8 | – | −10.4/7.6 | 7.7/54.1 | −53.6/147.0 | –/38.4 | – | −15.7/−7.7 |
| | STN | −80.7/−51.8 | −79.1/−50.7 | −8.9/30.1 | −73.4/−50.8 | −60.1/−5.6 | −60.7/16.7 | –/−40.8 | – | −72.8/−19.2 |
| | SEARCH | −42.3/−51.5 | −33.4/−21.8 | – | −25.2/−19.9 | −10.4/14.5[e] | −8.9/108.6 | –/31.2 | – | 4.7/−3.5 |
| 24-h avg. $NO_3^-$ | CASTNET | 28.3/282.7 | −45.6/129.7 | – | −56.8/106.5 | 24.1/69.7 | 5.3/275.6 | –/125.6 | – | −59.6/121.4 |
| | IMPROVE | 82.8/367.3 | −20.5/231.2 | 70.7/−63.6 | −34.6/197.8 | −39.4/−24.6 | 0.0/160.4 | –/159.9 | – | −41.9/89.7 |
| | STN | −41.9/3.3 | −64.8/−22.0 | 6.0/−54.4 | −69.4/−16.4 | −58.1/−34.7 | −46.2/42.9 | –/2.8 | – | −72.8/10.2 |
| | SEARCH | 58.6/604.5 | −22.0/444.6 | | −35.5/432.4 | −37.8/94.4[e] | 71.4/225.9 | –/127.4 | – | −35.0/127.8 |
| 24-h avg. $SO_4^{2-}$ | CASTNET | −45.5/−21.8 | −35.5/−11.8 | −48.4/41.9 | −25.9/−21.2 | −29.0/−3.0 | −26.6/51.9 | –/−8.3 | – | −8.5/−22.9 |
| | IMPROVE | −37.7/−14.5 | −42.4/−15.7 | −2.9/42.0 | −43.6/−23.5 | −21.4/−8.7 | 6.1/34.0 | –/−5.9 | – | −13.9/−17.9 |
| | STN | −70.3/−25.5 | −68.0/−26.6 | −40.0/52.7 | −62.5/−30.6 | −52.4/−4.6 | −58.7/12.7 | –/−20.2 | – | −42.9/−21.0 |
| | SEARCH | −29.0/−17.1 | −22.6/−8.8 | | −13.5/−10.6 | 28.8/17.5[e] | 16.0/76.2 | –/43.6 | – | 7.9/−5.4 |
| 24-h avg. BC | IMPROVE | 50.1/68.4 | 46.6/58.5 | 81.6/37.2 | 31.3/44.9 | 15.5/1.5 | 58.5/68.1 | –/31.7 | – | 20.1/3.6 |
| | SEARCH | −50.5/−40.5 | −46.5/−40.9 | | −32.9/−34.4 | −49.6/−54.1[e] | −7.0/−14.3 | –/−39.8 | – | −27.9/−45.1 |
| 24-h avg. OM | IMPROVE | 69.3/70.1 | 86.7/70.8 | 180.3/76.3[g] | 55.3/65.9 | 127.7/83.9[g] | 13.2/−37.1 | −21.3 | – | −0.3/43.4 |
| | SEARCH | −34.1/4.8 | −22.8/13.5 | | −15.6/4.0 | −39.2/−47.3[e,g] | 10.0/−49.4 | –/−36.1 | – | −15.7/2.2 |
| 24-h avg. TC | STN | −77.2/−37.3 | −73.4/−40.2 | −25.1/−31.1 | −66.3/−36.5 | – | – | –/42.7 | – | −55.0/−18.2 |
| Col. CO[h] | MOPITT | 10.0/20.1 | 9.9/31.1 | −8.4/– | 4.8/32.5 | −0.6/26.0 | 0.8/34.4 | –/−25.7 | 32.6/35.8 | 16.5/54.5 |
| Col. $NO_2$ | GOME | −0.5/−22.2 | 9.7/−23.7 | 19.4/−28.3 | −8.4/−30.6 | 21.9/−12.5 | 33.9/47.1 | –/5.1 | 33.0/−25.3 | −23.9/−33.9 |
| Col. $O_3$ | TOMS-SBUV | −9.9/−23.4 | 28.8/−46.9 | 8.9/−51.9 | 28.9/−53.2 | 26.3/−19.3 | 35.5/4.5 | –/−6.7 | 44.4/−52.2 | 67.2/−50.0 |

[a]All statistics are taken from *K. Wang et al.* [2009].
[b]All seasonal statistics are taken from *Zhang et al.* [2009a] and all Jan. and Jul. statistics are calculated in this work based on the simulations of *Zhang et al.* [2009a].
[c]All statistics are taken from *Zhang et al.* [2010a] using WRF/Chem version 2.2.
[d]All statistics are taken from *Zhang et al.* [2012a] using WRF/Chem-CB05-MADRID version 3.0.
[e]The seasonal-mean statistics is calculated for winter (December, January, and February) and summer (June, July, and August) in 2001.
[f]The statistics is obtained by comparing the average of Jan. and Jul. results in the boundary layer (0–400 m above ground level) with observed annual mean summarized in *Yu and Luo* [2009] (YL09). No statistics are calculated for D04 and D05 which contains only ≤2 data pairs.
[g]The statistics is calculated for OC.
[h]The statistics of column CO for summer is calculated based on the data in August. No data are available for June and July 2001.

over D01 in January and over all domains in July (NMBs of 106.5–282.7%, 89.7–367.3%, and 58.6–604.5%, respectively) but underpredicted over D02, D03, and D05 in January (NMBs of −59.6% to −45.6%, −41.9% to −20.5%, and −35.5% to −22.0%, respectively). The concentrations of EC and OM are overpredicted at the IMPROVE sites (NMBs of 3.6–68.4% and 43.4–86.7%, respectively) (except for OM over D05 in January) but underpredicted at the SEARCH sites (except for OM in July) in both months (NMBs of −50.5% to −27.9% and −34.1% to −15.6%, respectively). The concentrations of TC are largely underpredicted at the STN sites (NMBs of −77.2% to −18.2%), indicating possible underestimates in the emissions of EC and primary OM and concentrations of SOA. The overpredictions in the concentrations of EC, OM, and $NO_3^-$ at the IMPROVE and CASTNET sites help explain the overpredictions in $PM_{2.5}$ in both months, whereas the underpredictions in the concentrations of $NH_4^+$ and $SO_4^{2-}$ are mainly responsible for underpredictions of $PM_{2.5}$ at the STN sites over all domains in January and at the SEARCH sites over D01 and D02 in July. Column CO mass concentrations are overpredicted over all domains in both months (NMBs of 4.8–54.5% and NMEs of 11.9–54.5%). Column $NO_2$ mass concentrations are underpredicted over D01, D03, and D05 in January (NMBs of −23.9% to −0.5%) and over all domains in July (NMBs of −33.9% to −22.2%) but overpredicted over D02 and D05 in January (NMBs of 9.7–33.0%), with NMEs of 35.6–78.4% over all domains for both months. TOR is underpredicted over D01 in January and over all domains in July (NMBs of −53.2% to −9.8%), but overpredicted over D02–D05 in January (NMBs of 28.8–67.2%), with NMEs of 32.4–67.7% over all domains for both months. The biases in TOR are likely caused by the use of inaccurate upper boundary layer conditions for $O_3$ [*Zhang et al.*, 2009a]. For many species (e.g., $SO_2$, $NO_2$, $O_3$, $PM_{2.5}$, BC, and OM), the model bias generally reduces with successively finer domains, which demonstrates the benefit of using a progressively nested model from the global to local scale. For example, in July 2001 against AQS-AIRS, the NMBs for max 1-h $O_3$ mixing ratios over D01, D02, and D03 are −17.8, −16.7, and −10.5%, respectively, using the same sets of observations over D03 and those over D01, D02, D03, and D05 are −5.1, −4.4, −1.1, and 1.1%, respectively, using the same sets of observations over D05. The NMBs for 24-h average concentrations over D01, D02, D03, and D05 in July 2001 against IMPROVE are 44.6, 27.7, 18.2, and 6.0%, respectively. These results are consistent with those of *Jacobson* [2001b].

[31] Compared with regional model simulations using MM5/CMAQ over D02 [*K. Wang et al.*, 2009], GU-WRF/Chem performs much better or similarly for $PM_{2.5}$, OM, column CO, and column $NO_2$ at most sites in both months and some $PM_{2.5}$ components (e.g., $SO_4^{2-}$ at all sites in July and EC and $NO_3^-$ at the IMPROVE sites in January). It gives slightly worse performance for maximum 1-h and 8-h average $O_3$ and TC in both months, and inorganic PM components at the STN sites, some PM components such as $SO_4^{2-}$ at the IMPROVE sites and $NH_4^+$ at the CASTNET sites, $NO_3^-$ at the IMPROVE sites, and TOR in January. The differences in chemical predictions between GU-WRF/Chem and MM5/CMAQ over D02 are mainly due to differences in the emissions used over CONUS (the 1999 NEI version 1 for MM5/CMAQ and the 1999 NEI version 3 for GU-WRF/Chem) and in some meteorological predictions such as WS10 (i.e., much higher WS10 from WRF than from MM5). Compared with regional model simulations using MM5/CMAQ over D03 [*Zhang et al.*, 2009a], GU-WRF/Chem performs better for OM at all sites and EC at the SEARCH site in both months and column $NO_2$ and TOR in January. It gives slightly worse maximum 1-h and 8-h $O_3$ and worse $PM_{2.5}$ and most of its components in both months except for $PM_{2.5}$ at the IMPROVE and SEARCH sites. GU-WRF/Chem uses the same version of 1999 NEI version 3 as MM5/CMAQ over CONUS except for lower $NO_2$ emissions as mentioned previously. The lower $NO_x$ emissions used in GU-WRF/Chem simulations can explain lower concentrations of $O_3$, $PM_{2.5}$ and its components, and column $NO_2$. Compared with regional model simulations using mesoscale WRF/Chem (version 2.2) over D03 [*Zhang et al.*, 2010a], GU-WRF/Chem performs better for maximum 1-h and 8-h $O_3$ at most sites and column $NO_2$ in both months, TOR in January, as well as $PM_{2.5}$ and most of its components in July. It gives worse performance for $PM_{2.5}$ and most of its components in January and TOR in July. While the lower $NO_x$ emissions used in GU-WRF/Chem contribute largely to the differences in model predictions, other important factors include major updates in the model treatments in WRF/Chem v3.0 on which GU-WRF/Chem is based, as compared with WRF/Chem v2.2 used for the regional simulations. In particular, large overpredictions by WRF/Chem v2.2 are caused by two main problems. The first one is in the Yonsei University (YSU) PBL scheme that arbitrarily sets an unrealistic value of 15-m for nocturnal PBL height, leading to a lower PBL height that contributes to the nighttime overpredictions of $PM_{2.5}$ in both months [*Misenis and Zhang*, 2010]. This problem has been corrected in WRF/Chem v3.0 [*Hong et al.*, 2008] and thus, in GU-WRF/Chem. The second problem lies in the non-positive definite advection scheme used in the regional simulations because the positive definite advection scheme was not available in WRF/Chem v2.2. This may contribute to the large overpredictions in $PM_{2.5}$ and its composition in July at many sites in the eastern U.S., which are located near the large point sources of the gaseous precursors of secondary $PM_{2.5}$ or their downwind areas [*Chapman et al.*, 2009; *Zhang et al.*, 2010a]. Despite an overall better performance than WRF/Chem v2.2 in July, the GU-WRF/Chem performance is not as good as expected. A possible reason is the larger overprediction in Precip, which scavenges too much soluble $PM_{2.5}$ species such as $NH_4^+$ and $SO_4^{2-}$. The worse Precip predictions are caused by a coarser vertical resolution used in GU-WRF/Chem than that in WRF/Chem v2.2, i.e., the former uses 27 layers from surface to 50 mb (23 layers from surface to 100 mb) and the latter uses 34 layers from the surface to ∼100 mb, although the first model layer height for both models is set to be ∼40 m above the ground level (AGL). This is because the cumulus parameterization is very sensitive to the vertical resolution. A sensitivity simulation over D03 using the mesoscale WRF/Chem with the Grell-Devenyi cumulus parameterization [*Grell and Devenyi*, 2002] shows a worse performance using a coarser vertical resolution.

[32] Several bugs in WRF/Chem v2.2 and 3.0 were corrected based on the bug report at http://www.mmm.ucar.edu/wrf/users/wrfv3/known-prob.html. These include one bug in the Kain-Fritsch (KF) II scheme that may cause long-lasting

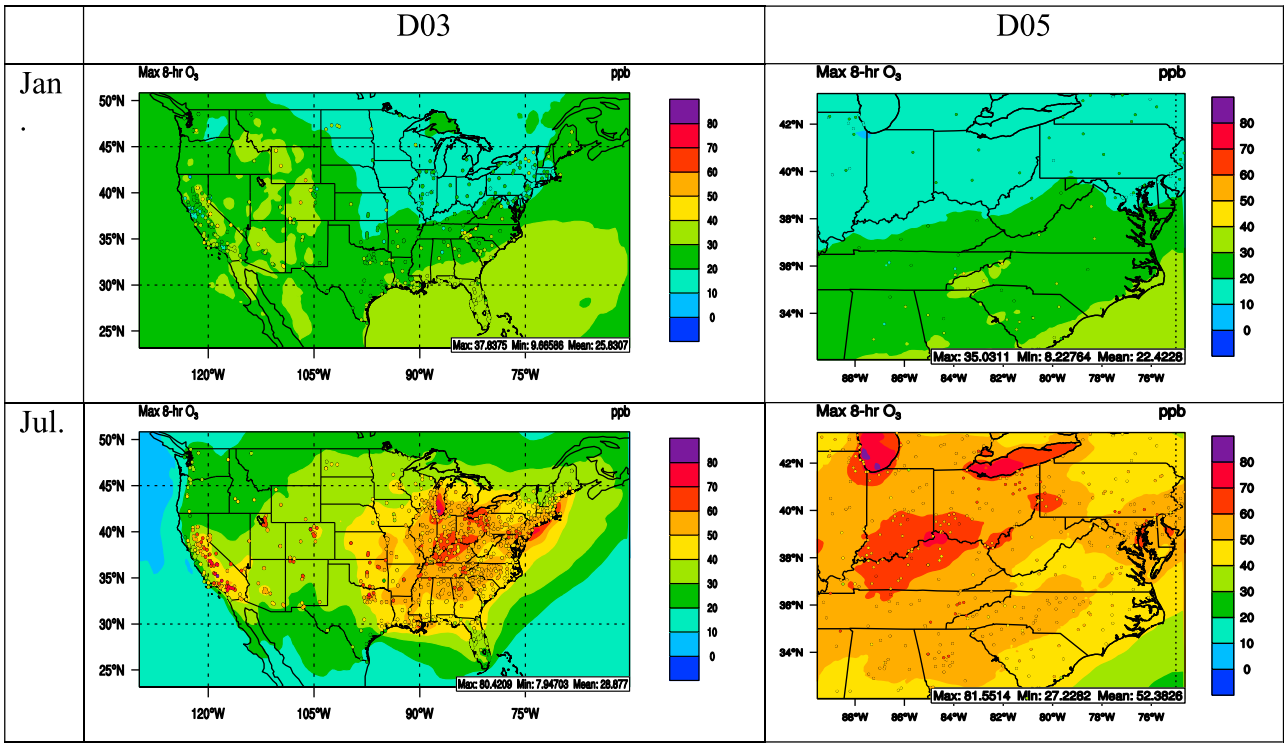


**Figure 5.** Simulated surface max. 8-h average $O_3$ mixing ratios overlaid with observations from CASTNET, AIRS-AQS, and SEARCH over D03 and D04.

cloud in rare areas and another bug in the Lin microphysics scheme that causes the overprediction of cloud ice, graupel, and surface rainfall. However, the mesoscale WRF/Chem-MADRID that is based on WRF/Chem v3.0 still overpredicts Precip. Comparing with regional model simulations using the mesoscale WRF/Chem-MADRID (v3.0) over D03 in July, GU-WRF/Chem performs either better or comparably for all gaseous species except for CO, maximum 1-h and 8-h $O_3$, column $NO_2$, and TOR, and aerosol species except for $NH_4^+$ at the CASTNET and IMPROVE sites, $NO_3^-$ and $SO_4^{2-}$ at most sites, and OM at the IMPROVE sites. Although Precip is less overpredicted by GU-WRF/Chem than by WRF/Chem-MADRID, the concentrations of some PM species such as $NH_4^+$ and $SO_4^{2-}$ are underpredicted to a larger extent, due to larger underpredictions of CDNC, CWP, and CF and thus underpredictions in aqueous-phase formation of $(NH_4)_2SO_4$.

[33] Figures 5 and 6 show the simulated surface mixing ratios of $O_3$ and concentrations of $PM_{2.5}$ overlaid with available observations from surface networks over CONUS (D02) and the eastern U.S. The underpredictions in the mixing ratios of $O_3$ occur mostly in the western U.S. in both months, and in the central plains and the eastern U.S. in July. Simulated $O_3$ mixing ratios at $0.08° \times 0.10°$ over D05 show more details in concentration gradients (e.g., a good agreement with observations over several high $O_3$ regions such as southern Indiana and northern Kentucky, and a few lower $O_3$ regions in southern South Carolina, eastern North Carolina, central Virginia, and eastern Pennsylvania where underpredictions occur in July that cannot be predicted at $0.33° \times 0.42°$ in D03). The use of a finer grid resolution greatly improves the agreement of model predictions with observations of surface $O_3$ in July although it degrades its performance slightly in January (see Table 2). The model captures several high $PM_{2.5}$ areas in the Midwest and the southeastern U.S. in both months, although it misses a few hot spots in the western and eastern U.S. in both months. The model simulates higher $PM_{2.5}$ concentrations with a greater gradient over several areas over D05 at $0.08° \times 0.10°$ than at $0.33° \times 0.42°$ in both months. The use of a finer grid resolution greatly improves the agreement of model predictions with observations of $PM_{2.5}$ in both months, in particular, at the STN sites in January and the IMPROVE sites in July (see Table 2).

[34] Figure 7 shows the global spatial distributions of predicted net concentrations of $PM_{10}$, $PM_{2.5}$, and $PM_{2.5}$ composition resulting from emissions and all formation paths but excluding contributions from boundary conditions in January and July, 2001. Those concentrations are obtained by taking the differences between the baseline simulations and the simulations in which PM emissions and formation processes for secondary PM are turned off. In January, $PM_{10}$ concentrations can be up to 268.8 $\mu g\ m^{-3}$ with a global mean of 19.7 $\mu g\ m^{-3}$. Over most land areas $PM_{2.5}$ constitutes over 80% of $PM_{10}$, except for a few deserts/arid regions where coarse PM dominates (e.g., Sahara deserts in northern Africa and Taklamakan and Gobi deserts in northwestern China). Sea-salt can dominate over the ocean, with concentrations of 10–50 $\mu g\ m^{-3}$ over most oceanic areas. $PM_{2.5}$ concentrations are high over regions where anthropogenic sources are significant. They are dominated by both inorganic and carbonaceous PM components in Asia, North America, and Europe but primarily carbonaceous PM in Africa due to high biomass burning emissions [*Roberts et al.*, 2009].

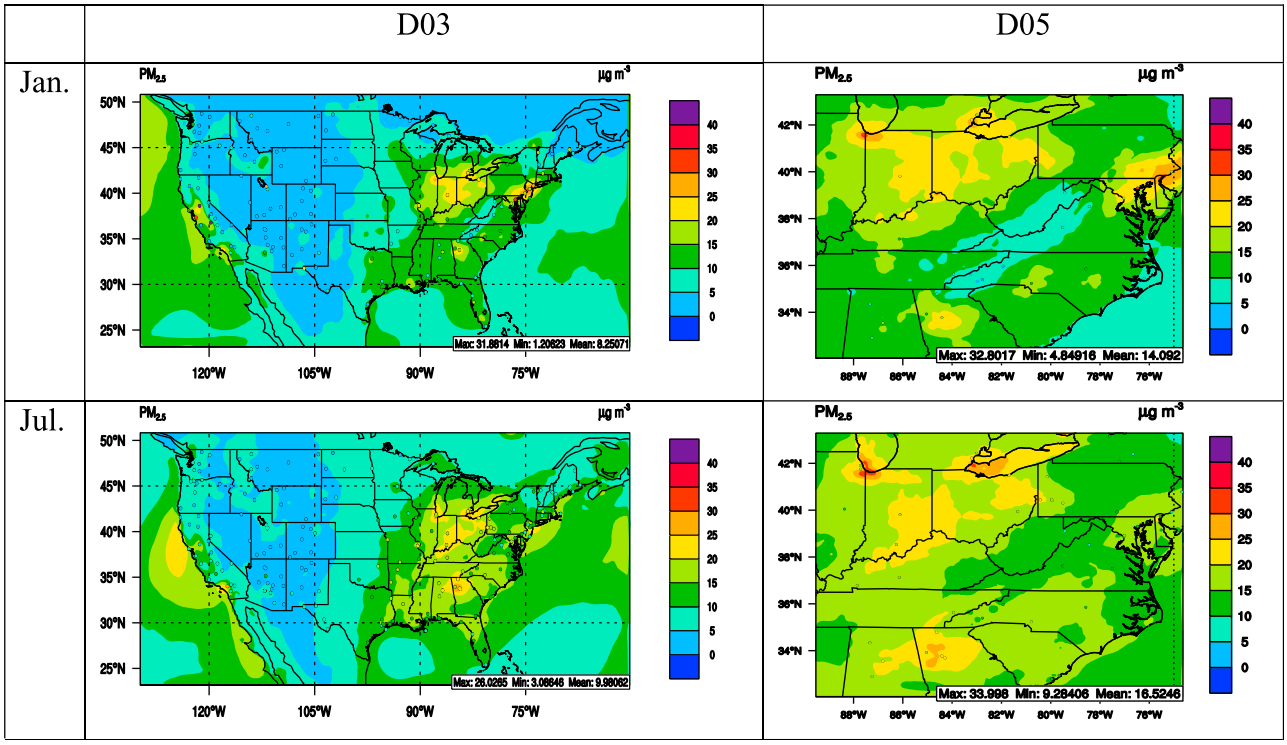


**Figure 6.** Simulated surface max. 24-h average $PM_{2.5}$ concentrations overlaid with observations from IMPROVE, STN, and SEARCH over D03 and D04.

Concentrations of $NO_3^-$ can be up to 10 $\mu$g m$^{-3}$, with a global mean of 0.8 $\mu$g m$^{-3}$. In July, $PM_{10}$ and $PM_{2.5}$ concentrations can be up to 248.3 and 246.7 $\mu$g m$^{-3}$ with a global mean of 19.4 and 9.9 $\mu$g m$^{-3}$, respectively, and $PM_{2.5}$ constitutes more than 90% of $PM_{10}$ over most land areas except for a few deserts/arid regions. Compared with January, the coarse PM concentrations over the Sahara deserts, the Arabian deserts in the Middle East, and the Taklamakan deserts are much higher. Sea-salt concentrations are also higher in the oceanic areas in the southern hemisphere (10–60 $\mu$g m$^{-3}$) due to stronger winds. While the $PM_{2.5}$ concentrations in Europe (in particular, Spain), South Asia, and eastern China are smaller, those in South Africa, eastern Europe, and the U.S. are larger in July, which are also consistent with the seasonal variations of observed $PM_{2.5}$ concentrations [e.g., *Zhang et al.*, 2009a; *Liu et al.*, 2010]. The concentrations of $SO_4^{2-}$ are much higher over all industrial continents where anthropogenic emissions of $SO_2$ are high and those of $NO_3^-$ are much lower due to high temperatures that do not favor its formation. The concentrations of EC and OM are much lower in Asia and much higher in southern Africa and northern South America, which are also consistent with other modeling and satellite studies (e.g., the work of *Roberts et al.* [2009] in Africa).

### 3.5. Aerosol Feedbacks

[35] Figures 8 and 9 show the effect of $PM_{2.5}$ on meteorological and chemical predictions through direct, semi-direct, and indirect effects in January and July, respectively. In January, the regions with large changes in meteorological and cloud-related variables correlate with those having high $PM_{10}$ concentrations (see Figure 7) or large percentage changes (figure not shown). $PM_{10}$ reduces SWDOWN in most areas by up to 83.1 W m$^{-2}$ (−55.5%) with a global average of 17.2 W m$^{-2}$ (−7.5%). The areas of reduction generally follow the spatial distribution of $PM_{10}$. It reduces LWDOWN over regions with high $PM_{10}$ concentrations such as central Africa and eastern China by up to 5.8 W m$^{-2}$ (−1.6%), although the global average is a net increase of 0.9 W m$^{-2}$ (0.3%), due to enhanced LWDOWN in regions where $PM_{10}$ concentrations are relatively low but the warming effect of greenhouse gases and EC dominates. As a direct response to reduced SWDOWN, the photolysis rates of $NO_2$ decrease by up to 2.1 × 10$^{-3}$ s$^{-1}$ (−68.9%), with a global mean reduction of 2.2 × 10$^{-4}$ s$^{-1}$ (−9.3%). T2 is affected by many factors including radiation, land-air surface fluxes, and boundary processes through semi-direct effects, with a net reduction by 1°C (−2693.8%) over regions with high $PM_{10}$ concentrations and a global mean reduction of 0.05°C (−1.4%), whereas RH2 increases by up to 4.6% (7.7%) with a global mean increase of 0.2% (0.3%). As shown in Figure 10, the decreases in temperatures extend from the surface to the boundary layers (<800 mb) due to the dominance of backscattering of solar radiation by aerosols but they either increase slightly or remain unchanged at higher latitudes due to the increased infrared radiation caused by absorbing aerosols such as black carbon that dominates over or offsets the cooling caused by aerosol backscattering in January. PBL height decreases by up to 262 m (−28.3%) over regions with high $PM_{10}$ concentrations, with a global mean decrease of 5.9 m (−1.0%). WS10 and Precip decrease slightly by up to 0.3 m s$^{-1}$ (−11.5%) and 3.9 mm day$^{-1}$ (−79.4%) over these regions, with a global mean of −0.006 m s$^{-1}$ (−0.2%) and −0.002 mm day$^{-1}$ (−0.1%). As

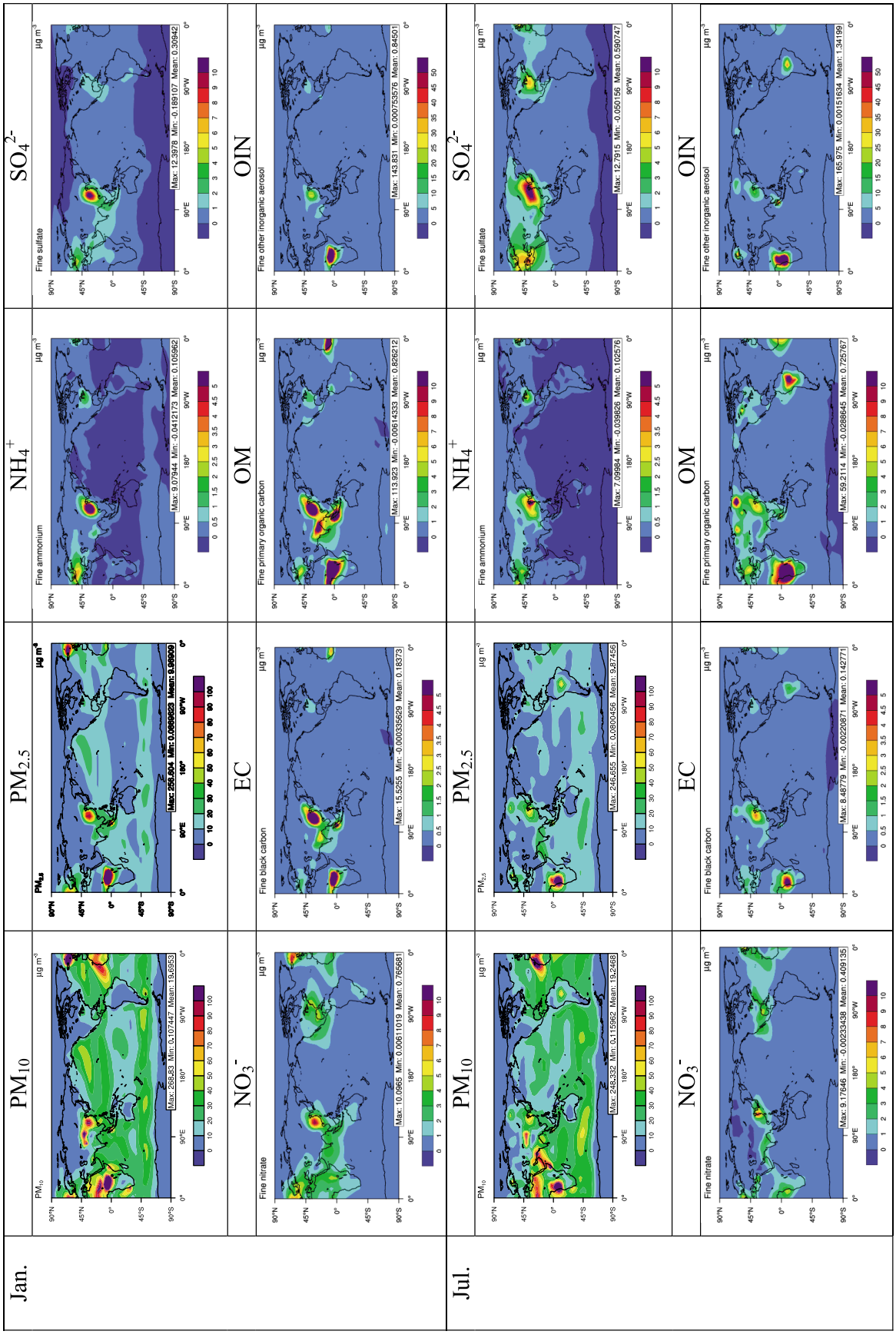


**Figure 7.** The surface concentrations of $PM_{10}$, $PM_{2.5}$, and $PM_{2.5}$ composition by GU-WRF/Chem produced from emissions and secondary aerosol formation pathways in Jan. and Jul., 2001.

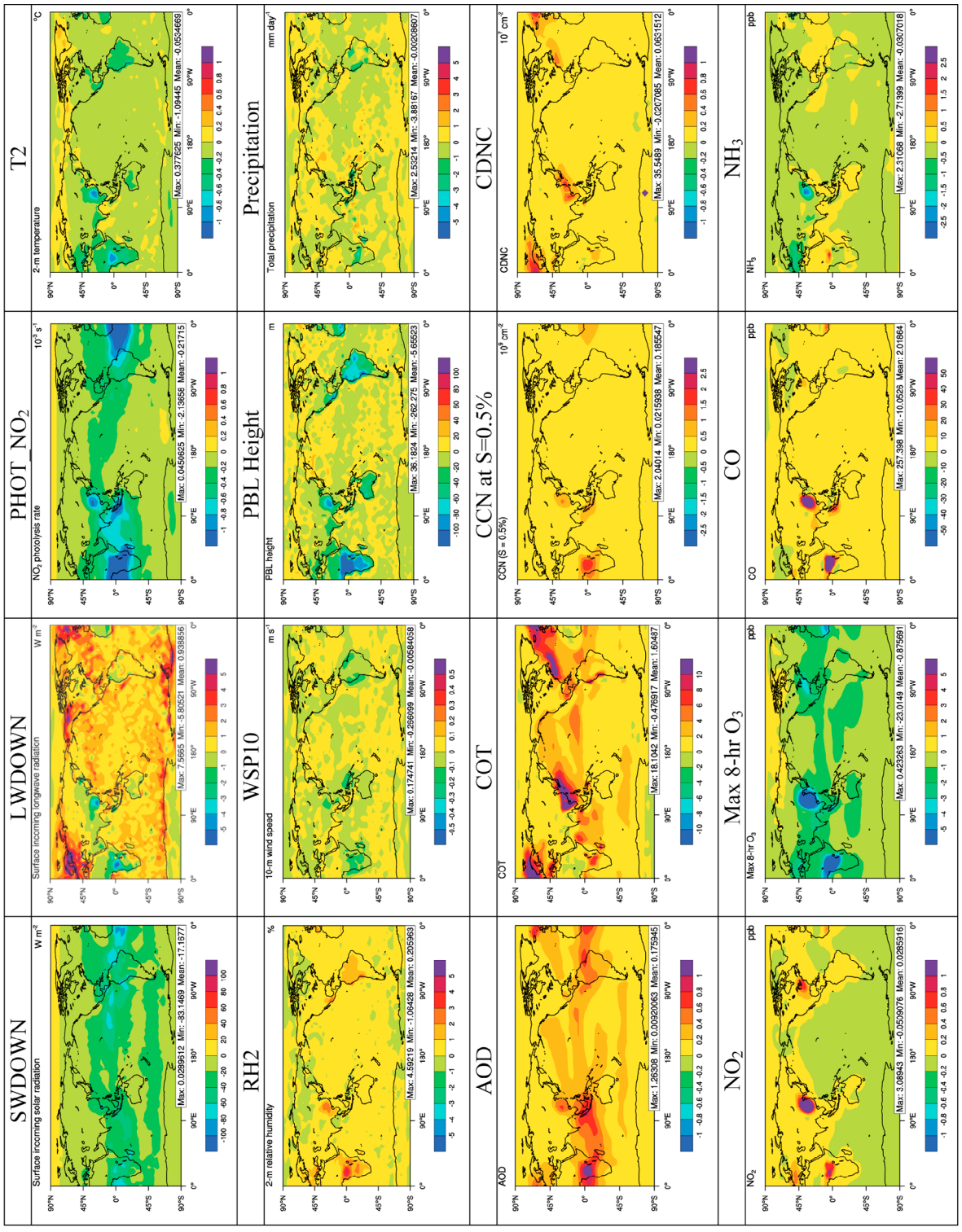


**Figure 8.** Simulated effects of $PM_{10}$ on meteorological and chemical variables on a global scale in January 2001 obtained by taking differences between simulation results with PM and without PM emissions and processes. The mixing ratios of $NO_2$, max 8-h $O_3$, CO, and $NH_3$ shown are at surface.

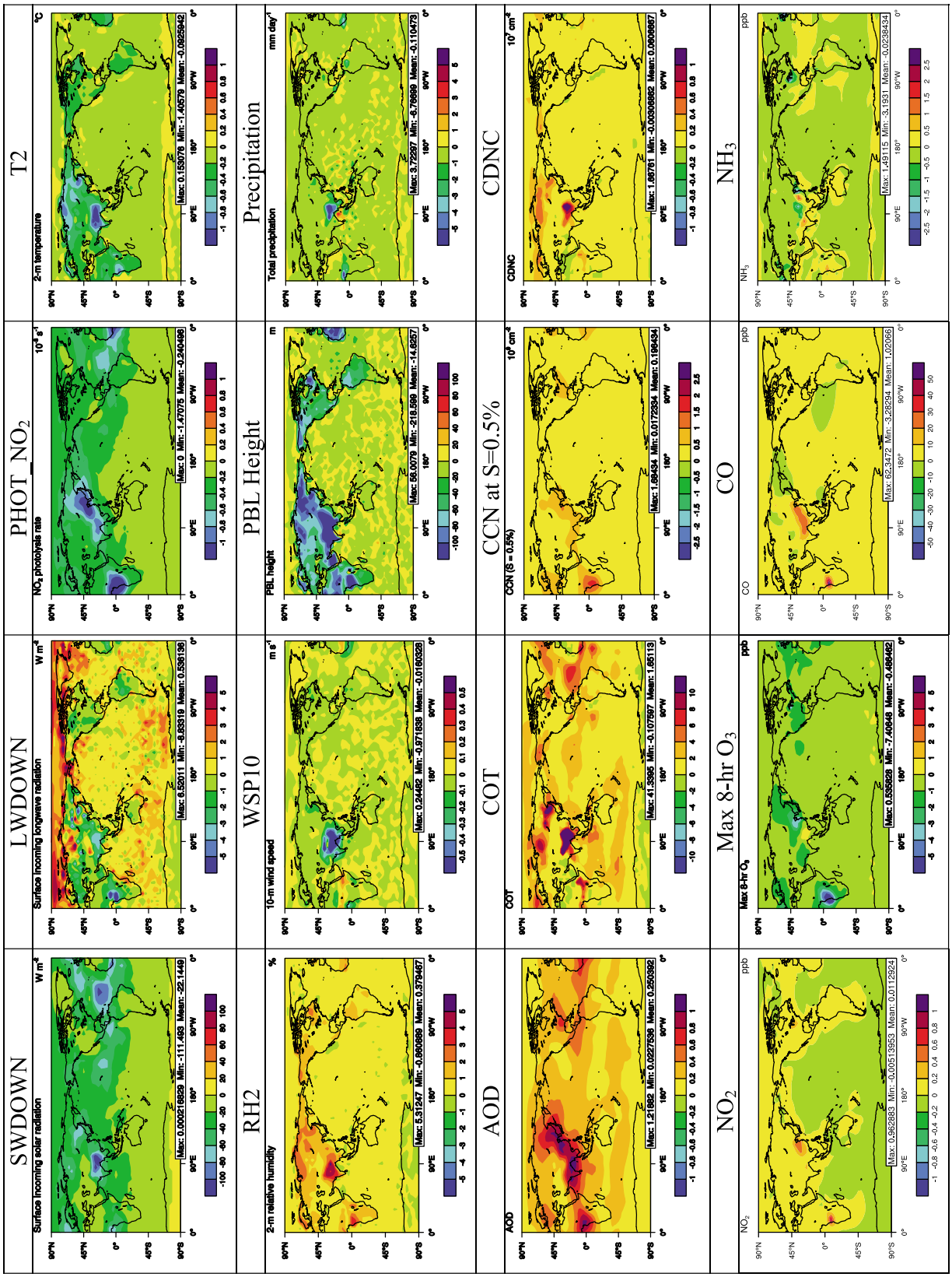


**Figure 9.** Simulated effects of $PM_{10}$ on meteorological and chemical variables on a global scale in July 2001 obtained by taking differences between simulation results with PM and without PM emissions and processes. The mixing ratios of $NO_2$, max 8-h $O_3$, CO, and $NH_3$ shown are at surface.

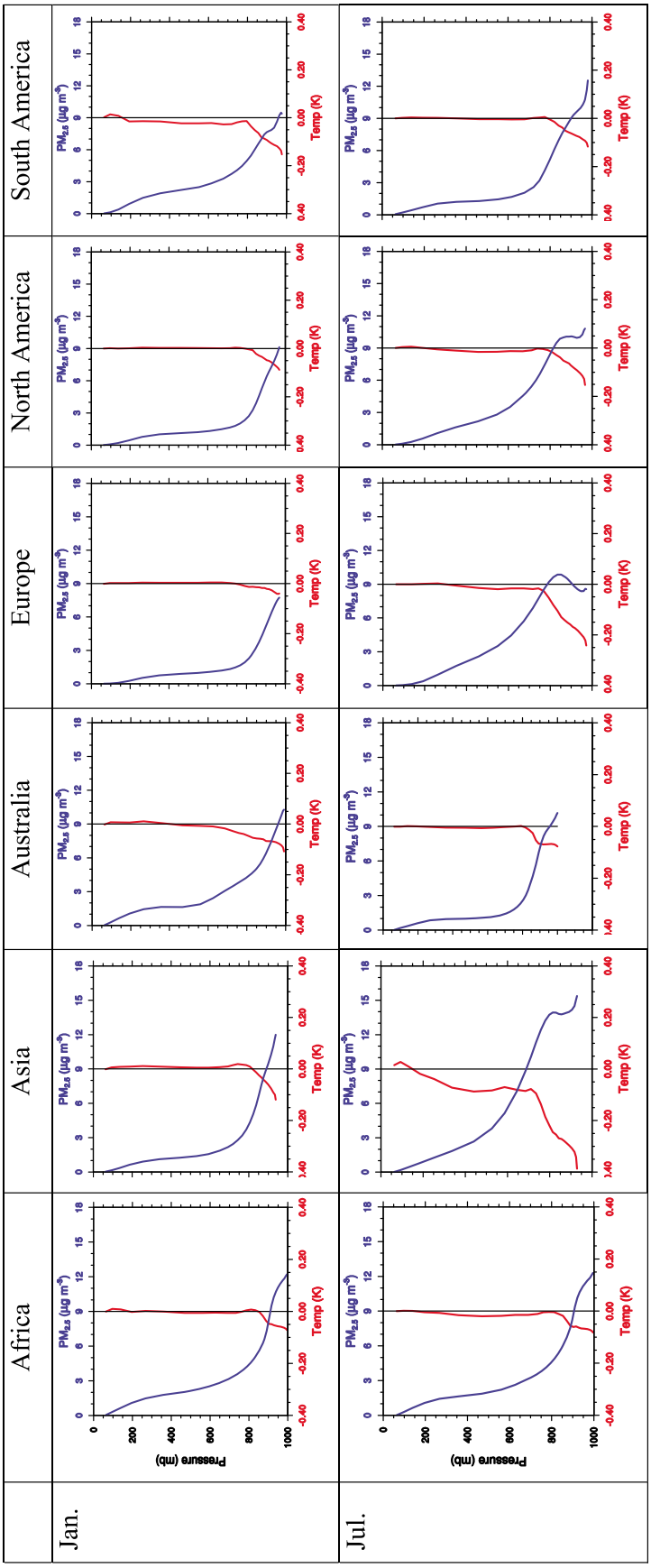


**Figure 10.** Vertical profiles of $PM_{2.5}$ and temperatures over six populated continents.

expected, AOD and column CCN at supersaturation (S) of 0.5% increase throughout the globe by up to 1.26 (12631%) and $2.0 \times 10^9$ cm$^{-2}$ (3671%) with a global mean of 0.17 (4772%) and $1.9 \times 10^8$ cm$^{-2}$ (506%), respectively. CF increases through indirect effect of $PM_{2.5}$ throughout the globe with a global mean of 67.4%. COT follows the pattern of $PM_{2.5}$ and increases by up to 18.1 (2204%) in most areas with a global mean of 1.6 (104%). Column CDNC also increases by up to $3.5 \times 10^8$ cm$^{-2}$ (by 355489%) in nearly all areas, with a global mean of $8.3 \times 10^5$ cm$^{-2}$ (433%), because of aerosol indirect effects. The changes in meteorological and radiative variables affect the distributions and magnitudes of chemical species. As a consequence of decreased SWDOWN and $NO_2$ photolysis rates, the surface mixing ratios of $NO_2$ increase by up to 3 ppb (67.2%) with a global mean of 0.029 ppb (8.5%), and the surface mixing ratios of OH and $HO_2$ radicals reduce by up to 0.07 (−72.6%) and 7.1 ppt (−64.2%) with a global mean reduction of $4.8 \times 10^{-3}$ (−13.9%) and 0.42 (−9.4%) ppt (figures not shown), which in turn leads to a decrease in surface $O_3$ mixing ratios by up to 23 ppb (−45.6%) with a global mean reduction of 0.9 ppb (−5.6%). $PM_{2.5}$ also affects slowly reacting or nonreactive species such as CO and $NH_3$ by affecting atmospheric stability and total oxidation capacity. As shown in Figures 8 and 9, the surface mixing ratios of CO increase by up to 257.4 ppb (12.6%) with a global mean increase of 2 ppb (1.8%) over most areas as a result of decreased OH, reduced WS10, and reduced PBL height. The changes in the mixing ratio of $NH_3$ can occur in either direction. For example, it decreases in eastern Asia and Europe where a large amount of $NH_4^+$ forms, driving $NH_3$ from the gas-phase to the particulate phase, which dominates over the increase in $NH_3$ mixing ratio caused by a reduced PBL height. The mixing ratio of $NH_3$ increases in northern Africa where the effect of a reduced PBL height dominates over that due to the formation of a small amount of $(NH_4)_2SO_4$.

[36] In July, the variation trends for the above variables and concentrations are overall similar to those in January, although they differ in their spatial distributions and magnitudes due to a different spatial distribution of $PM_{2.5}$ in July. Larger reductions occur in SWDOWN by up to 111.5 W m$^{-2}$ (−45.0%), photolysis of $NO_2$ by up to $1.5 \times 10^{-3}$ s$^{-1}$ (−52.3%), T2 by up to −1.4°C (−546.6%), WS10 by up to 1.0 m s$^{-1}$ (−19.5%), PBL height by up to 218.6 m (−36.9%), and Precip by up to −6.8 mm day$^{-1}$ (−82.0%), with global means of −22.1 W m$^{-2}$ (−10.8%), $-2.4 \times 10^{-4}$ s$^{-1}$ (−11.6%), −0.09°C (−1.1%), −0.016 m s$^{-1}$ (−0.4%), −14.6 m (−2.2%), and −0.1 mm day$^{-1}$ (−4.6%), respectively. Similar to January, the decreases in temperatures occur in the low portion of the atmosphere but temperatures either increase slightly or remain unchanged at higher altitudes (<800 mb) over all major continents except for Asia where the reduction in temperatures occurs up to 100 mb (see Figure 10). Similarly, the increases in RH2, AOD, COT, and column CCN are larger in July than in January. Although CF is higher in July than in January, the increase in the column CDNC in July is slightly smaller, because WRF/Chem v3.0 does not treat the activation of particles by convective clouds that often occurs in July. The increase in $NO_2$ mixing ratios is smaller in July than in January, because of the losses of $NO_2$ with higher destruction rates of $NO_2$ for all chemical reactions other than the $NO_2$ photolytic reaction that offset some of the gain through the reduced $NO_2$ photolysis rate and PBL height under summer conditions. The decrease in the surface mixing ratios of $O_3$ is also smaller, by up to 7.4 ppb (−18.5%) with a global mean reduction of 0.5 ppb (−3.2%), due to a smaller reduction in the surface mixing ratios of OH and $HO_2$ radicals (by up to 0.05 and 4.0 ppt with a global mean reduction of $3.6 \times 10^{-3}$ (−10.1%) and 0.44 (−8.0%) ppt, respectively). Despite larger decreases in WS10 and PBL height in July than in January, the increase in the surface mixing ratios of CO is also smaller in July because of a smaller decrease in the surface mixing ratios of OH under summer conditions. As for the January case, the changes in the surface mixing ratio of $NH_3$ can occur in either direction in July, although the magnitudes of the changes are smaller, because of a stronger compensation effect of reduced PBL height that tends to increase $NH_3$ and aerosol thermodynamics that tends to decrease $NH_3$.

[37] The use of a finer horizontal grid resolution captures additional spatial variability. This is demonstrated in Figure 11, which compares spatial distributions of $PM_{10}$ effects on simulated RH2, WS10, COT, Precip, and the mixing ratios of $NH_3$ over D04, D03, and D05 in July. Compared with results at a grid resolution of 4° × 5° (see Figure 8), the use of a grid resolution of 0.33° × 0.42° gives higher increases in RH2 in central China, opposite changes in WS10 (increases rather than decreases) in southwestern China, higher increases in COT and larger decreases in Precip in southern China but smaller increases in COT and smaller decreases in Precip in southwestern China, and larger decreases in $NH_3$ mixing ratios in central China. Compared with results over the eastern U.S. at a grid resolution of 0.33° × 0.42° (D03) shown in Figure 11, the use of a grid resolution of 0.08° × 0.10° (D05) shows somewhat different areas with higher increases in RH2 in some states (e.g., Ohio), larger areas of decreases in WS10 in South Carolina and North Carolina, greater increases in COT in South Carolina and southeastern West Virginia, greater reductions in Precip along the Blue Ridge Mountains, and greater reductions in $NH_3$ mixing ratios in the state of West Virginia and along the Blue Ridge Mountains.

## 4. Sensitivity Studies

[38] Figure 12 shows spatial distributions of simulated surface PM number concentrations from the baseline simulation (with the binary homogeneous nucleation algorithm of *McMurry and Friedlander* [1979]) and sensitivity simulations using alternative nucleation (SI06 and YU10) and aerosol activation (FN05) parameterizations. Figure 13 shows the vertical distributions of simulated PM number concentrations, CCN at S of 0.5%, and CDNC from these simulations. Simulated surface PM number concentrations are very sensitive to nucleation parameterizations. The simulation with SI06 gives high surface PM number concentrations with a global mean of $6.63 \times 10^3$ cm$^{-3}$ at the surface (which is a factor of 4.8 higher than the global mean of $1.39 \times 10^3$ cm$^{-3}$ from the baseline simulation) and throughout the vertical domain. Since SI06 is derived based on observations at a rural region with large areas of forested land at a 73-m high tower during springtime when nucleation events frequently occur and the empirical prefactor of

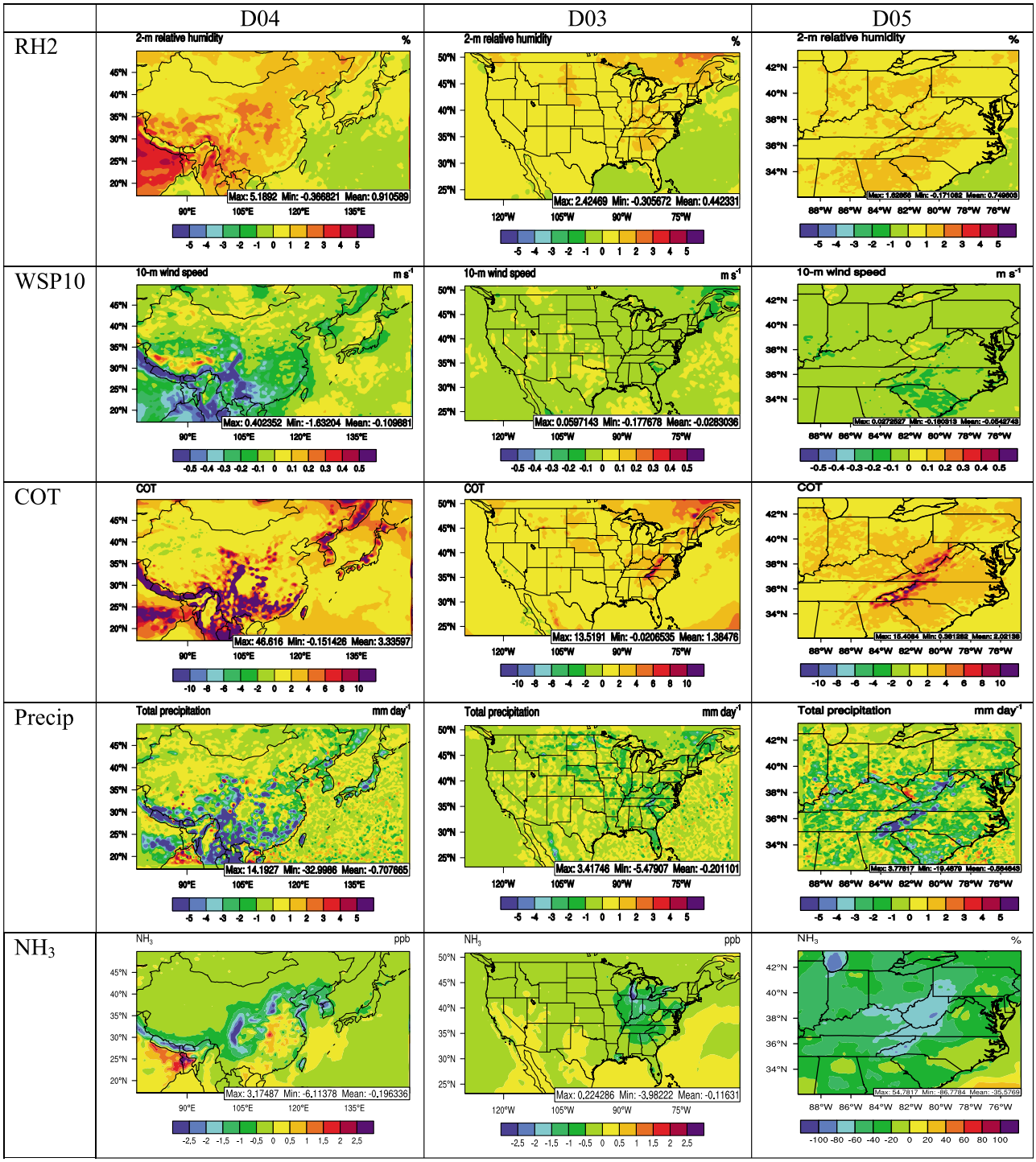


**Figure 11.** Simulated effects of $PM_{10}$ on meteorological and chemical variables on urban and regional scale in July 2001 obtained by taking differences between simulation results with PM and without PM emissions and processes. The mixing ratios of $NH_3$ shown are at surface.

SI06 does not vary with temperature (as well as other factors known to affect nucleation), it tends to give higher nucleation rates and PM number concentrations under other cleaner conditions in other regions. The simulation with YU10 gives surface PM number concentrations with a global mean of $1.28 \times 10^3$ cm$^{-3}$ that is 7.7% lower than the baseline value at the surface but higher PM number concentrations above 650 mb, likely as a result of different nucleation rates predicted by two different nucleation models (associated with different underlying physics and thermodynamic data of the two nucleation models). Differences in aerosol mass and number concentrations further lead to sizable differences in simulated CCN and CDNC due to the feedback mechanisms among $H_2SO_4$ vapor, $PM_{10}$ number,

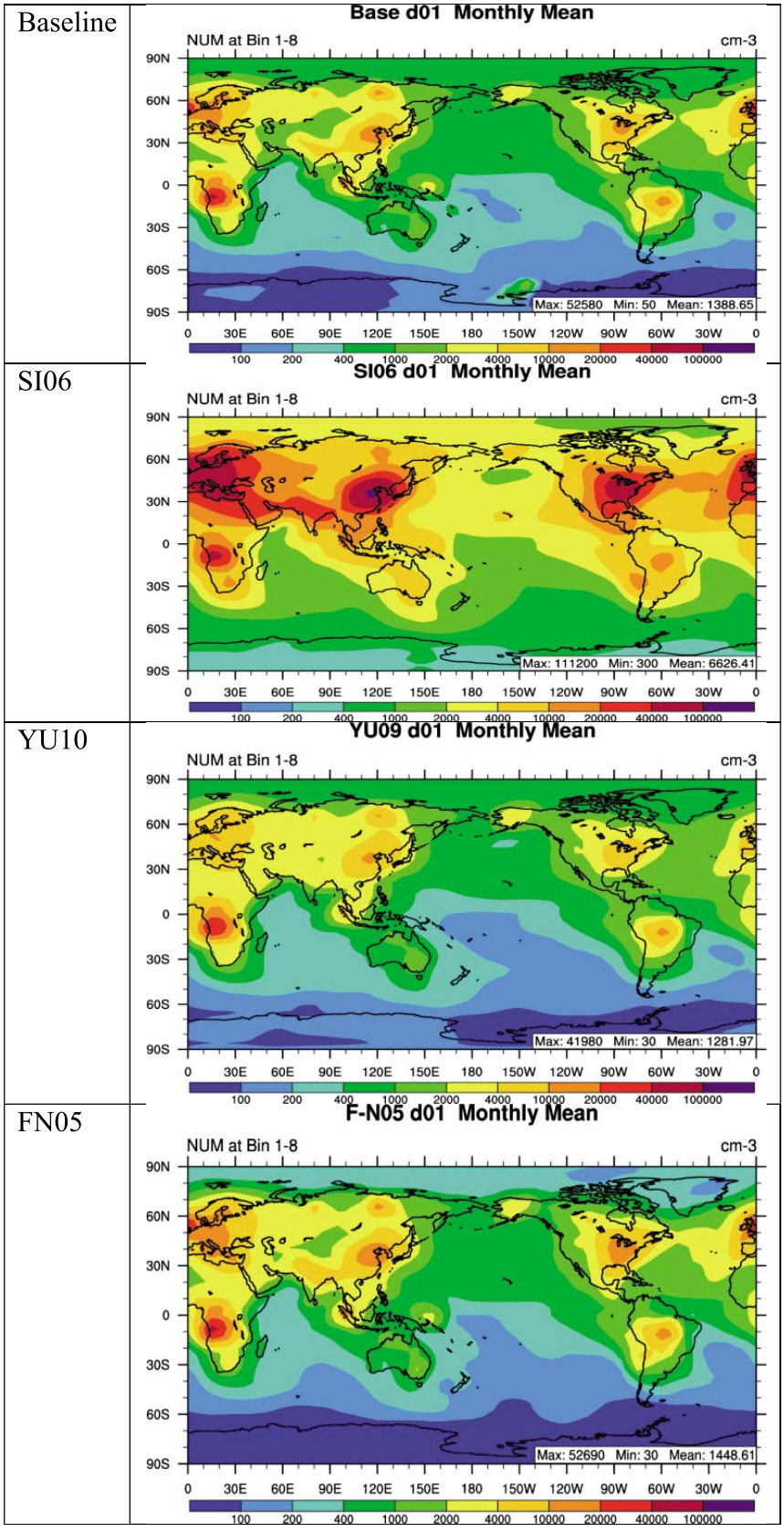


**Figure 12.** Simulated total PM number concentrations ($cm^{-3}$) at surface in July 2001 from baseline and sensitivity simulations.

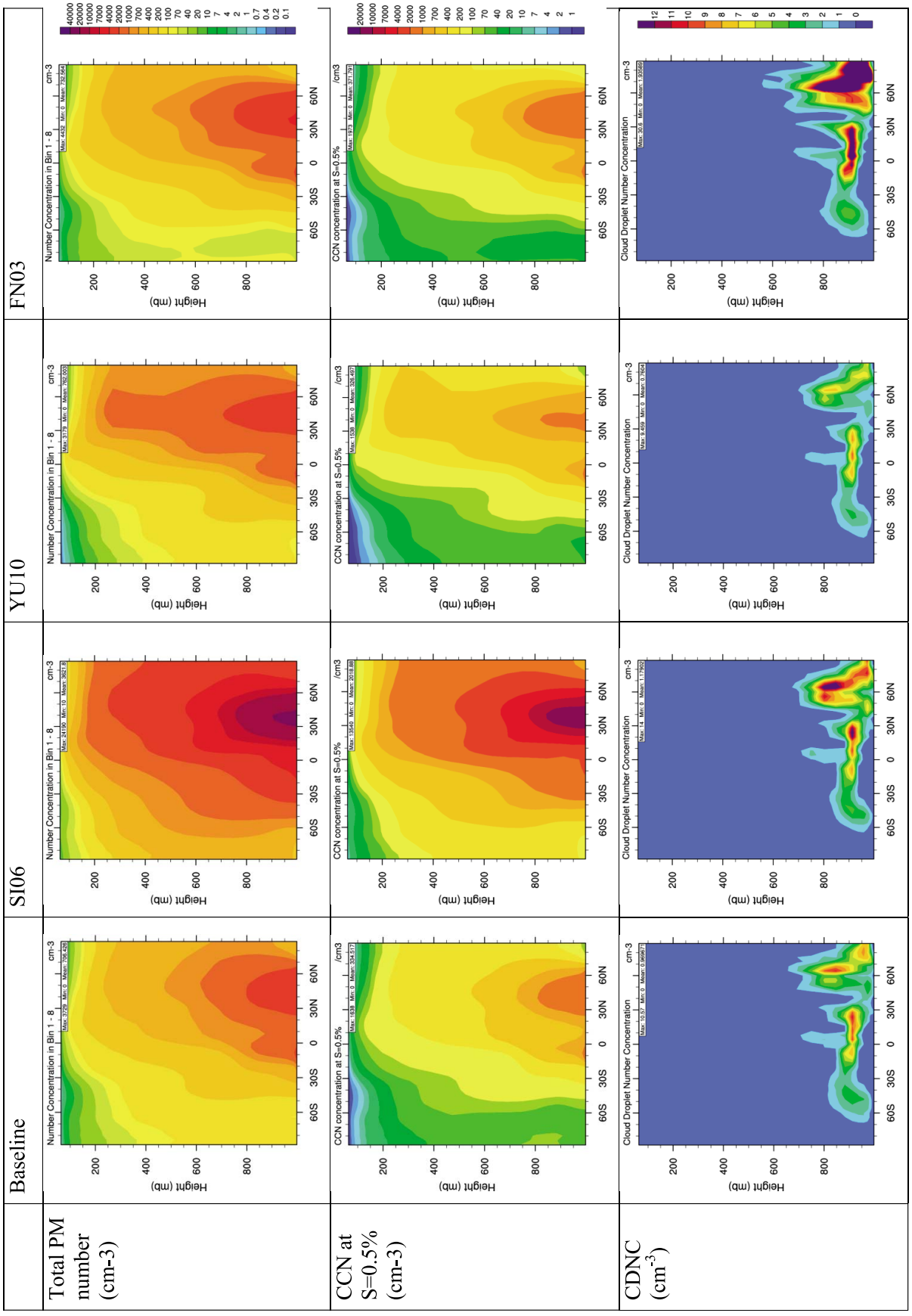


**Figure 13.** Simulated vertical total PM number concentrations, CCN at S = 0.5%, and CDNC in July 2001 from baseline and sensitivity simulations.

CCN, and CDNC through gas-phase chemistry, new particle formation, aerosol growth, and aerosol activation by cloud droplets.

[39] As shown in Figure 13, the simulation with FN05 gives slightly higher PM number concentrations with a global mean of $1.45 \times 10^3$ cm$^{-3}$ (which is higher by 4.1% than the baseline value) at the surface and in the vertical domain, indicating a small sensitivity of PM number concentrations to the aerosol activation scheme. The simulated CCN concentrations at S of 0.5% correlate well with the simulated PM number concentrations, i.e., the simulation with SI06 gives the highest CCN throughout the atmosphere among all simulations, the simulation with YU10 gives lower CCN below 850 mb but higher CCN above 850 mb than the baseline simulation, and the simulation with FN05 gives a vertical distribution of CCN that is similar to the baseline simulation but slightly higher in magnitude. In contrast to the simulated PM number and CCN concentrations that are more sensitive to nucleation parameterizations, simulated CDNC is much more sensitive to the aerosol activation parameterization. Among the four simulations, the simulation with FN05 gives the highest CDNC between 1000 and 600 mb (i.e., mostly warm clouds), followed by the simulation with SI06, the baseline simulation, and the simulation with YU10. CDNC in WRF/Chem is a strong function of CCN. The CCN spectrum is determined as a function of PM number concentrations using the Kőhler theory, following the aerosol activation/resuspension parameterization of *Abdul-Razzak and Ghan* [2002] used in the baseline simulation and that of *Fountoukis and Nenes* [2005] used in the simulation with FN05. Under certain circumstances, the kinetic effect considered in FN05 may slow the growth of CCN (compared to the equilibrium approach of ARG02) and increase the number of CDNC, since $S_{max}$ increases As $S$ increases, the differences between the two parameterizations become smaller because more and more aerosol activates and CDNC becomes insensitive to $S_{max}$ errors (figures not shown). The higher CDNC predicted by FN05 in Figure 13 is primarily due to the different values of the uptake coefficient used in FN05 (0.06) and ARG02 (1.0). Several other differences in the treatments between FN05 and ARG02 may also be responsible for differences in the predictions. For example, ARG02 neglects size-dependence of the water vapor diffusivity coefficient which may lead to an underestimate of CDNC. As a result, FN05 gives higher activation fractions than ARG02 for a given temperature, pressure, updraft velocity, and CCN spectrum, leading to higher CDNC. These results are consistent with the comparison between the older versions of the ARG02 and FN05 modules [e.g., *Ghan et al.*, 2011]. Since CCN depends primarily on PM number concentrations and CDNC depends strongly on CCN, the simulation with SI06 gives higher CDNC than the simulation with YU10 and the baseline simulation because of higher PM number and CCN, when the same aerosol activation parameterization of ARG02 is used for these three simulations.

[40] Figure 14 shows simulated zonal-mean total PM mass and number concentrations and several radiative properties including AOD, OLR, outgoing shortwave radiation (OSR), SWDOWN, and several cloud properties including CF, COT, CWP, CCN at a supersaturation of 0.5%, CDNC, and cloud effective radius (CER). Available observations of AOD, OLR, CF, COD, and CCN from MODIS and CDNC from *Bennartz* [2007] are also plotted for comparison. All simulations overpredict AOD, with the best agreement by the simulation with FN05 in the northern hemisphere. All simulations reproduce the observed OLR zonal mean profile reasonably well with similar overpredictions in the tropics; they give very similar zonal profiles of OSR and SWDOWN. All simulations significantly underpredict COT and CDNC in all latitude bands and CF except for the regions between 60 and 90° where overprediction occurs. All simulations overpredict CCN at $S$ of 0.5%. While OLR, OSR, SWDOWN, and CF are relatively insensitive to nucleation and aerosol activation parameterizations, other variables exhibit moderate to high sensitivity to these parameterizations. The simulation with SI06 gives the lowest zonal mean $PM_{10}$ mass and the highest $PM_{10}$ number and CCN concentrations. The simulation with FN05 gives similar zonal mean profile of $PM_{10}$ mass concentrations as the other two simulations but lower $PM_{10}$ number concentrations at higher latitudes. It also gives lower AOD and CWP and much higher CER over most latitude bands, higher COT between 60 and 90°, and higher CDNC between 45 and 90° than all other three simulations. Higher CDNC would result in a higher cloud reflectivity, and consequently higher COTs. Lower CDNC between −50 and 45° and higher CDNC between 45 and 90° by the simulation with FN05 lead to higher and lower CER for clouds below 600 mb in these latitude bands, respectively.

## 5. Conclusions and Future Work

[41] A global-through-urban WRF/Chem model with online-coupled meteorology and chemistry and consistent model treatments at all scales has been developed to provide a unified model framework to simulate the chemistry-aerosol-cloud-radiation-precipitation-climate feedbacks across scales. Despite moderate to large model biases in some simulated meteorological and chemical variables, GU-WRF/Chem demonstrates promising capability in reproducing observations of many variables that are comparable or even better than the mesoscale models such as WRF/Chem and MM5/CMAQ. The main reasons for model biases in meteorological predictions are attributed to current model limitations in simulating cloud microphysics, in particular, convective clouds, and the PBL and land-surface processes, and the lack of some feedback mechanisms (e.g., no coupling between the Kain-Fritsch (II) scheme and radiation and between cumulus parameterizations and aerosol activation schemes). The main reasons for model biases in chemical predictions are attributed to inaccurate emissions of primary PM and secondary PM precursors and inaccurate meteorological predictions (e.g., overpredictions in SWDOWN and Precip in both months). The use of a coarse horizontal grid resolution may also be responsible for model biases for some variables, because clouds and other subgrid processes cannot be resolved and the emissions cannot be well represented. The use of higher resolutions in nested domains can generally improve the model performance of the predictions of these variables (e.g., SWDOWN, T2, WD10, RH2, $O_3$, and $PM_{2.5}$).

[42] Aerosols can feed back to radiation, meteorology, and cloud microphysics at all scales. Aerosols decrease the magnitudes of a number of variables. These variables include shortwave radiation, $NO_2$ photolysis rate, near-

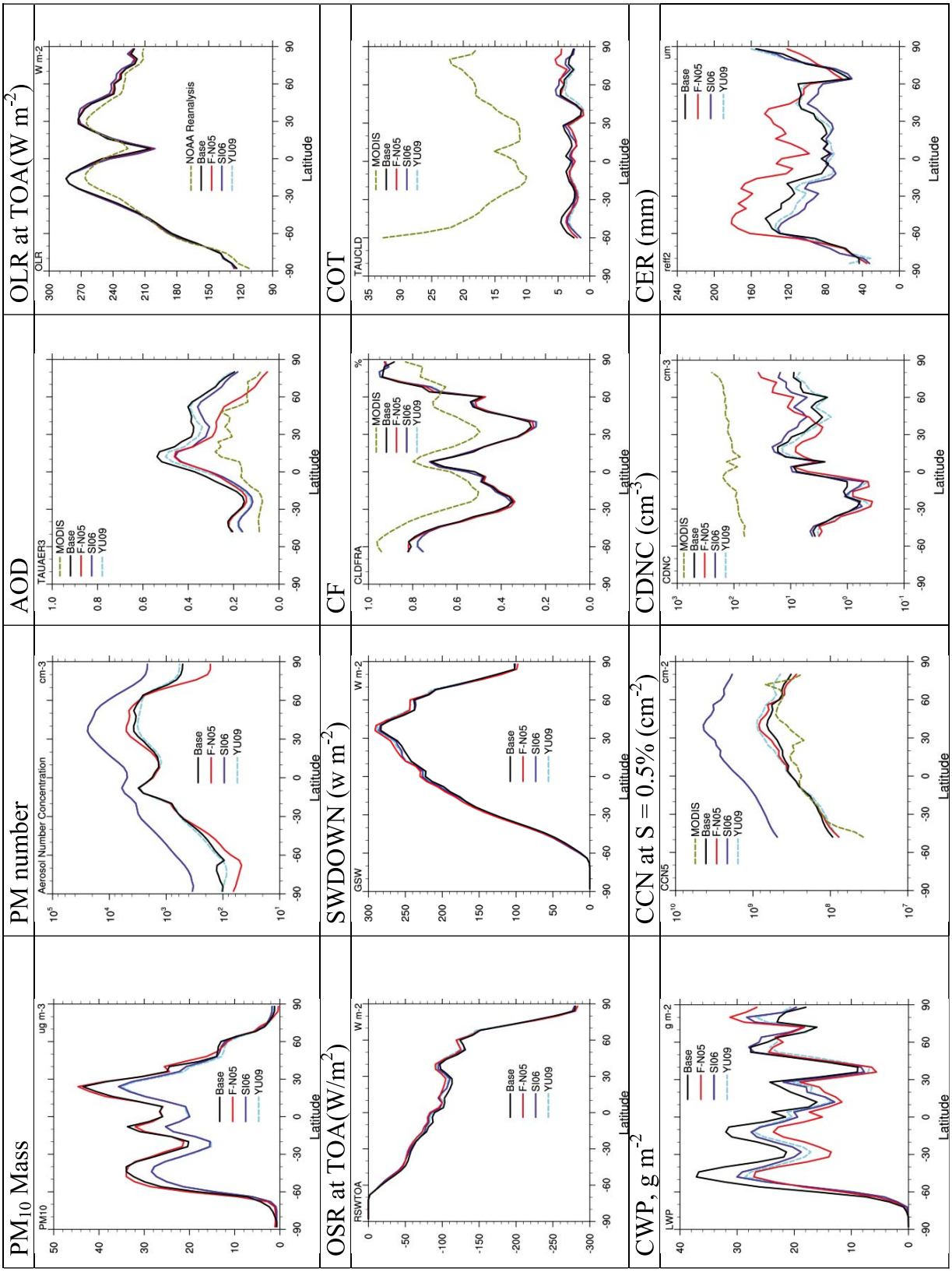


**Figure 14.** Simulated zonal-mean (averaged over all longitudes) total PM mass and number concentrations, radiative and cloud properties in July 2001 from baseline and sensitivity simulations CCN at S = 0.5%, and CDNC in July 2001 from baseline and sensitivity simulations.

surface temperature, WS10, PBL height and precipitation, with global mean decreases of 17.2–22.1 W $m^{-2}$ (−9.9% to −8.7%), 2.2 × $10^{-4}$ to 2.4 × $10^{-4}$ $s^{-1}$ (−10.7% to −10.5%), 0.05–0.09°C (−2% to −1.6%), 0.006 to 0.016 m $s^{-1}$ (−0.4% to −0.2%), 5.9–14.6 m (−1.7% to −0.9%) and 0.002–0.1 mm $day^{-1}$ (−5% to −1%), respectively. Aerosols also reduce LWDOWN by up to 5.8–8.8 W $m^{-2}$ (−2.2% to −1.6%), although there is a net increase of 0.5–0.9 W $m^{-2}$ (0.2–0.3%) in the global average value. Aerosols increase the magnitudes of several variables. These variables include RH2, AOD, column CCN at *S* of 0.5%, COT, CDNC, with global mean increases of 0.2–0.4% (0.3–0.6%), 0.17–0.25 (1759.5–2503.9%), 1.9 × $10^8$ to 2.0 × $10^8$ $cm^{-2}$ (488.3–546.8%), 1.6–1.65 (80.2–83.6%), and 6.0 × $10^5$ to 8.3 × $10^5$ $cm^{-2}$ (317.7–476%), respectively. Such feedbacks also change the spatial distribution, abundance, and lifetimes of reactive and non-reactive chemical species through changing radiation, atmospheric stability, photolysis rates, chemical reaction rates, total oxidation capacity, and the rates of all meteorological-dependent chemical and microphysical processes for $O_3$ and PM formation. The use of a finer horizontal grid resolution captures spatial variability of aerosol feedbacks that cannot be captured at a coarser grid resolution. Simulated aerosol, radiation, and cloud properties exhibit small-to-high sensitivity to different nucleation and aerosol activation parameterizations. Among all variables examined, PM mass and number concentrations, CCN, and Precip show a higher sensitivity to nucleation parameterizations, while AOD, COT, CDNC, LWP, and CER show a higher sensitivity to activation parameterizations, and OLR, GLW, GSW, SWDOWN, RSWTOA, and CF show a small sensitivity to nucleation and aerosol activation parameterizations.

[43] Several limitations exist for this study. First, all simulations shown in this work use one-way nesting, and do not include the feedbacks of changes in the meteorological and chemical fields at urban scales to larger scales which requires two-way nesting. Second, GU-WRF/Chem does not treat all meteorology-chemistry feedbacks at present due primarily to the limitations in the understanding of such feedback mechanisms (e.g., the aerosol activation by convective cloud droplets and the effect of convection clouds on radiation are not included in WRF/Chem v3.0). It will thus undergo continuous model development to become a more mature model. Third, one caveat is that the advection scheme is inconsistent between the global and nested domains. While the positive definition and monotonic advection scheme is used in the nested domain, this scheme does not work for the global configuration because its formulation depends on the requirement that Courant numbers should be less than 1, a condition which, cannot be met in the atmosphere in the region of the poles (W. C. Skamarock, NCAR, personal communications, 2010). At present, there is no easy way to simulate positive-definite transport that is conservative on the latitude-longitude grid in a finite-volume formulation. Therefore, the 5th order horizontal momentum advection and the 3rd order vertical momentum advection schemes are used for D01. Finally, GU-WRF/Chem does not explicitly resolve stratospheric dynamics and only simulates a limited number of stratospheric chemical reactions. As a result, the model exhibits some numerical instabilities over polar regions and upper model layers, causing high concentrations of $O_3$ and a buildup of mass concentrations of nitrate in those regions and layers. However, the use of the chemistry polar filter developed by NCAR in all the simulations in this work greatly reduced numerical instability of $O_3$ in polar regions. A smaller time step for advection processes was used to help converge the numerical solution, which reduced most nitrate buildup.

[44] Nevertheless, GU-WRF/Chem represents one of the few unified global-through-urban models with consistent model treatments (except for the advection scheme between D01 and smaller domains) that can be applicable to simulate air quality and its interactions with meteorology and climate across a wide range of the spatial scales, quantify such interactions, study the relative importance of major atmospheric processes, and assess the effectiveness of $O_3$ and PM attainment under different future climate and emission scenarios. Similar to traditional source apportionment that has been used to guide the development of emission control strategies, an apportionment of aerosol feedbacks can provide valuable speciated feedbacks that can be used to guide the development of the optimal emission control strategies for both air quality control and adverse climate change mitigation.

[45] **Acknowledgments.** This project is sponsored by the EPA STAR grant R83337601 and the China's National Basic Research Program (2010CB951803). AN acknowledges support from NASA MAP and NSF CAREER. Thanks are due to Mark Richardson at Caltech and William C. Skamarock at NCAR, for developing global WRF and sharing it with the community; William C. Skamarock at NCAR for helpful discussions; Louisa Emmons and Francis Vitt at NCAR for providing CAM4 and MOZART4 emissions; Christian Seigneur and Kristen Lohman, formerly at Atmospheric and Environmental Research, Inc., for providing global mercury emissions; Jerome Fast, Steve Ghan, Richard Easter, and Rahul Zaveri at PNNL, for public release of PNNL's version of WRF/Chem; Ken Schere, Golam Sarwar, and Shawn Roselle, U.S. EPA, for providing CB05 and CB05Cltx and Shaocai Yu, U.S. EPA, for providing Fortran code for statistical calculations; and Jack Fishman and John K. Creilson at NASA LRC, for providing TOR data. Thanks are also due to the contributions of former and current members of the air quality forecasting laboratory at NCSU including Xin-Yu Wen, Ying Pan, Yao-Sheng Chen, Kai Wang, and Xin Zhang.

## References

Abdul-Razzak, H., and S. J. Ghan (2002), A parameterization of aerosol activation. 3. Sectional representation, *J. Geophys. Res.*, *107*(D3), 4026, doi:10.1029/2001JD000483.

Ackermann, I. J., H. Hass, M. Memmesheimer, A. Ebel, F. S. Binkowski, and U. Shankar (1998), Modal aerosol dynamics model for Europe: Development and first applications, *Atmos. Environ.*, *32*, 2981–2999, doi:10.1016/S1352-2310(98)00006-5.

Bennartz, R. (2007), Global assessment of marine boundary layer cloud droplet number concentration from satellite, *J. Geophys. Res.*, *112*, D02201, doi:10.1029/2006JD007547.

Brasseur, G. P., and E. Roeckner (2005), Impact of improved air quality on the future evolution of climate, *Geophys. Res. Lett.*, *32*, L23704, doi:10.1029/2005GL023902.

Cangialosi, J. P., S. S. Chen, and J. Michalakes (2005), Hurricane simulations using a vortex-following nested grid in MM5 and WRF, paper presented at 2005 Joint WRF/MM5 User's Workshop, Mesoscale and Microscale Meteorol. Div., Natl. Cent. for Atmos. Res., Boulder, Colo., 27–30 June.

Chapman, E. G., W. I. Gustafson Jr., R. C. Easter, J. C. Barnard, S. J. Ghan, M. S. Pekour, and J. D. Fast (2009), Coupling aerosol-cloud-radiative processes in the WRF-Chem model: Investigating the radiative impact of elevated point sources, *Atmos. Chem. Phys.*, *9*, 945–964, doi:10.5194/acp-9-945-2009.

Chen, F., and J. Dudhia (2001), Coupling an advanced land surface-hydrology model with the Penn State-NCAR MM5 modeling system. Part I: Model implementation and sensitivity, *Mon. Weather Rev.*, *129*, 569–585.

Chen, S. H., and W. Y. Sun (2002), A one-dimensional time dependent cloud model, *J. Meteorol. Soc. Jpn.*, *80*, 99–118, doi:10.2151/jmsj.80.99.

Chen, W. T., A. Nenes, H. Liao, P. J. Adams, J. F. Li, and J. H. Seinfeld (2010), Global climate response to anthropogenic aerosol indirect effects: Present day and year 2100, *J. Geophys. Res.*, *115*, D12207, doi:10.1029/2008JD011619.

Chou, M. D., M. J. Suarez, C. H. Ho, M. M. H. Yan, and K. T. Lee (1998), Parameterizations for cloud overlapping and shortwave single-scattering properties for use in general circulation and cloud ensemble models, *J. Clim.*, *11*, 202–214, doi:10.1175/1520-0442(1998)011<0202:PFCOAS>2.0.CO;2.

Chuang, C. C., J. E. Penner, K. E. Taylor, A. S. Grossman, and J. J. Walton (1997), An assessment of the radiative effects of anthropogenic sulfate, *J. Geophys. Res.*, *102*, 3761–3778, doi:10.1029/96JD03087.

Chung, S. H., and J. H. Seinfeld (2005), Climate response of direct radiative forcing of anthropogenic black carbon, *J. Geophys. Res.*, *110*, D11102, doi:10.1029/2004JD005441.

Dentener, F. J., G. R. Carmichael, Y. Zhang, J. Lelieveld, and P. J. Crutzen (1996), Role of mineral aerosol as a reactive surface in the global troposphere, *J. Geophys. Res.*, *101*, 22,869–22,889, doi:10.1029/96JD01818.

Done, J. M., L. R. Leung, C. A. Davis, and B. Kuo (2005), Simulation of warm season rainfall using regional climate model, paper presented at 2005 Joint WRF/MM5 User's Workshop, Mesoscale and Microscale Meteorol. Div., Natl. Cent. for Atmos. Res., Boulder, Colo., 27–30 June.

Draxler, R. R., D. A. Gillette, J. S. Kirkpatrick, and J. Heller (2001), Estimating $PM_{10}$ air concentrations from dust storms in Iraq, Kuwait, and Saudi Arabia, *Atmos. Environ.*, *35*, 4315–4330, doi:10.1016/S1352-2310(01)00159-5.

Ek, M. B., K. E. Mitchell, Y. Lin, E. Rogers, P. Grunmann, V. Koren, G. Gayno, and J. D. Tarpley (2003), Implementation of Noah land surface model advances in the National Centers for Environmental Prediction operational mesoscale Eta model, *J. Geophys. Res.*, *108*(D22), 8851, doi:10.1029/2002JD003296.

Emmons, L. K., et al. (2010), Description and evaluation of the Model for Ozone and Related chemical Tracers, version 4 (MOZART-4), *Geosci. Model Dev.*, *3*, 43–67, doi:10.5194/gmd-3-43-2010.

Fahey, K. M., and S. N. Pandis (2001), Optimizing model performance: Variable size resolution in cloud chemistry modeling, *Atmos. Environ.*, *35*, 4471–4478, doi:10.1016/S1352-2310(01)00224-2.

Fast, J. D., W. I. Gustafson Jr., R. C. Easter, R. A. Zaveri, J. C. Barnard, E. G. Chapman, G. A. Grell, and S. E. Peckham (2006), Evolution of ozone, particulates, and aerosol direct radiative forcing on the vicinity of Houston using a fully coupled meteorology-chemistry-aerosol model, *J. Geophys. Res.*, *111*, D21305, doi:10.1029/2005JD006721.

Feichter, J., E. Roeckner, U. Lohmann, and B. Liepert (2004), Nonlinear aspects of the climate response to greenhouse gas and aerosol forcing, *J. Clim.*, *17*, 2384–2398, doi:10.1175/1520-0442(2004)017<2384:NAOTCR>2.0.CO;2.

Feser, F., and H. von Storch (2008), A dynamical downscaling case study for typhoons in SE Asia using a regional climate model, *Mon. Weather Rev.*, *136*, 1806–1815, doi:10.1175/2007MWR2207.1.

Fiore, A. M., D. J. Jacob, B. D. Field, D. G. Streets, S. D. Fernandes, and C. Jang (2002), Linking ozone pollution and climate change: The case for controlling methane, *Geophys. Res. Lett.*, *29*(19), 1919, doi:10.1029/2002GL015601.

Forkel, R., J. Werhahn, A. B. Hansen, S. McKeen, S. Peckham, G. Grell, and P. Suppan (2011), Effect of aerosol-radiation feedback on regional air quality—A case study with WRF/Chem, *Atmos. Environ.*, *53*, 202–211, doi:10.1016/j.atmosenv.2011.10.009.

Fountoukis, C., and A. Nenes (2005), Continued development of a cloud droplet formation parameterization for global climate models, *J. Geophys. Res.*, *110*, D11212, doi:10.1029/2004JD005591.

Gery, M. W., G. Z. Whitten, J. P. Killus, and M. C. Dodge (1989), A photochemical kinetics mechanism for urban and regional scale computer modeling, *J. Geophys. Res.*, *94*, 12,925–12,956, doi:10.1029/JD094iD10p12925.

Ghan, S. J., L. R. Leung, R. C. Easter, and H. Abdul-Razzak (1997), Prediction of cloud droplet number in a general circulation model, *J. Geophys. Res.*, *102*, 21,777–21,794, doi:10.1029/97JD01810.

Ghan, S. J., R. C. Easter, J. Hudson, and F. M. Breon (2001), Evaluation of aerosol indirect radiative forcing in MIRAGE, *J. Geophys. Res.*, *106*, 5317–5334, doi:10.1029/2000JD900501.

Ghan, S. J., H. Abdul-Razzak, A. Nenes, Y. Ming, X. Liu, M. Ovchinnikov, B. Shipway, N. Meskhidze, J. Xu, and X. Shi (2011), Droplet nucleation: Physically based parameterization and comparative evaluation, *J. Adv. Model. Earth Syst.*, *3*, M10001, doi:10.1029/2011MS000074.

Gillette, D. A., and R. Passi (1988), Modeling dust emission caused by wind erosion, *J. Geophys. Res.*, *93*, 14,233–14,242, doi:10.1029/JD093iD11p14233.

Giorgi, F., and C. Shields (1999), Tests of precipitation parameterizations available in the latest version of the NCAR regional climate model (RegCM) over continental U.S, *J. Geophys. Res.*, *104*, 6353–6375, doi:10.1029/98JD01164.

Gong, S., L. A. Barrie, and J. P. Blanchet (1997), Modeling sea salt aerosols in the atmosphere: 1. Model development, *J. Geophys. Res.*, *102*, 3805–3818, doi:10.1029/96JD02953.

Grell, G. A., and A. Baklanov (2011), Integrated modeling for forecasting weather and air quality: A call for fully coupled approaches, *Atmos. Environ.*, *45*, 6845–6851, doi:10.1016/j.atmosenv.2011.01.017.

Grell, G. A., and D. Devenyi (2002), A generalized approach to parameterizing convection combining ensemble and data assimilation techniques, *Geophys. Res. Lett.*, *29*(14), 1693, doi:10.1029/2002GL015311.

Grell, G. A., S. E. Peckham, R. Schmitz, S. A. McKeen, G. Frost, W. C. Skamarock, and B. Eder (2005), Fully coupled "online" chemistry within the WRF model, *Atmos. Environ.*, *39*, 6957–6975, doi:10.1016/j.atmosenv.2005.04.027.

Grell, G. A., J. Fast, W. I. Gustafson, S. E. Peckham, S. A. McKeen, M. Salzmann, and S. Freitas (2011a), On-line chemistry within WRF: Description and evaluation of a state-of-the-art multiscale air quality and weather prediction model, in *Integrated Systems of Meso-Meteorological and Chemical Transport Models*, edited by A. Baklanov, A. Mahura, and R. Sokhi, pp. 41–54, Springer, Heidelberg, Germany, doi:10.1007/978-3-642-13980-2_3.

Grell, G. A., S. R. Freitas, M. Stuefer, and J. D. Fast (2011b), Inclusion of biomass burning in WRF-Chem: Impact of wildfires on weather forecasts, *Atmos. Chem. Phys.*, *11*, 5289–5303, doi:10.5194/acp-11-5289-2011.

Guenther, A., P. Zimmerman, P. Harley, R. Monson, and R. Fall (1993), Isoprene and monoterpene emission rate variability: Model evaluation and sensitivity analysis, *J. Geophys. Res.*, *98*, 12,609–12,617, doi:10.1029/93JD00527.

Guenther, A., P. Zimmerman, and M. Wildermuth (1994), Natural volatile organic compound emission rate estimates for U.S. woodland landscapes, *Atmos. Environ.*, *28*, 1197–1210, doi:10.1016/1352-2310(94)90297-6.

Guenther, A., et al. (1995), A global model of natural volatile organic compound emissions, *J. Geophys. Res.*, *100*, 8873–8892, doi:10.1029/94JD02950.

Hogrefe, C., B. Lynn, K. Civerolo, J. Y. Ku, J. Rosenthal, C. Rosenzweig, R. Goldberg, S. Gaffin, K. Knowlton, and P. L. Kinney (2004), Simulating changes in regional air pollution over the eastern United States due to changes in global and regional climate and emissions, *J. Geophys. Res.*, *109*, D22301, doi:10.1029/2004JD004690.

Hong, S., Y. Noh, and J. Dudhia (2006), A new vertical diffusion package with an explicit treatment of entrainment processes, *Mon. Weather Rev.*, *134*, 2318–2341, doi:10.1175/MWR3199.1.

Hong, S. Y., S. W. Kim, J. Dudhia, and M. S. Koo (2008), Stable boundary layer mixing in a vertical diffusion package, paper presented at 9th Annual WRF Workshop, Natl. Cent. for Atmos. Res., Boulder, Colo., 23–27 June.

Intergovernmental Panel on Climate Change (IPCC) (2000), *Special Report on Emission Scenarios (SRES), A Special Report of Working Group III of the Intergovernmental Panel on Climate Change*, edited by N. Nakicenovic and R. Swart, 570 pp., Cambridge Univ. Press, Cambridge, U. K.

Intergovernmental Panel on Climate Change (IPCC) (2007), *Climate Change 2007: Synthesis Report. Contribution of Working Groups I, II and III to the Fourth Assessment Report of the Intergovernmental Panel on Climate Change, Core Writing Team*, edited by R. K. Pachauri and A. Reisinger, 104 pp., Geneva, Switzerland.

Jacobson, M. Z. (2001a), GATOR-GCMM: A global- through urban-scale air pollution and weather forecast model: 1. Model design and treatment of subgrid soil, vegetation, roads, rooftops, water, sea, ice, and snow, *J. Geophys. Res.*, *106*, 5385–5401, doi:10.1029/2000JD900560.

Jacobson, M. Z. (2001b), GATOR-GCMM: 2. A study of day- and nighttime ozone layers aloft, ozone in national parks, and weather during the SARMAP Field Campaign, *J. Geophys. Res.*, *106*, 5403–5420, doi:10.1029/2000JD900559.

Jacobson, M. Z. (2002), Control of fossil-fuel particulate black carbon plus organic matter, possibly the most effective method of slowing global warming, *J. Geophys. Res.*, *107*(D19), 4410, doi:10.1029/2001JD001376.

Jacobson, M. Z. (2004), The climate response of fossil-fuel and biofuel soot, accounting for soot's feedback to snow and sea ice albedo and emissivity, *J. Geophys. Res.*, *109*, D21201, doi:10.1029/2004JD004945.

Jacobson, M. Z. (2005), *Fundamentals of Atmospheric Modeling*, 2nd ed., 813 pp., Cambridge Univ. Press, New York, doi:10.1017/CBO9781139165389.

Jacobson, M. Z. (2008), Effects of wind-powered hydrogen fuel cell vehicles on stratospheric ozone and global climate, *Geophys. Res. Lett.*, *35*, L19803, doi:10.1029/2008GL035102.

Jacobson, M. Z., R. P. Turco, E. J. Jensen, and O. B. Toon (1994), Modeling coagulation among particles of different composition and size, *Atmos. Environ.*, *28*, 1327–1338, doi:10.1016/1352-2310(94)90280-1.

Jacobson, M. Z., Y. J. Kaufmann, and Y. Rudich (2007), Examining feedbacks of aerosols to urban climate with a model that treats 3-D clouds with aerosol inclusions, *J. Geophys. Res.*, *112*, D24205, doi:10.1029/2007JD008922.

Janjic, Z. I. (2002), Nonsingular implementation of the Mellor-Yamada level 2.5 scheme in the NCEP Meso model, *NCEP Off. Note, 437*, 61 pp., Natl. Cent. for Environ. Predict., College Park, Md.

Johnson, C. E., D. S. Stevenson, W. J. Collins, and R. G. Derwent (2001), Role of climate feedback on methane and ozone studied with a coupled Ocean-Atmosphere-Chemistry model, *Geophys. Res. Lett.*, *28*(9), 1723–1726, doi:10.1029/2000GL011996.

Kain, J. S. (2004), The Kain-Fritsch convective parameterization: An update, *J. Appl. Meteorol.*, *43*(1), 170–181.

Kain, J. S., and J. M. Fritsch (1990), A one-dimensional entraining/detraining plume model and its application in convective parameterization, *J. Atmos. Sci.*, *47*(23), 2784–2802.

Kain, J. S., and J. M. Fritsch (1993), Convective parameterization for mesoscale models: The Kain-Fritcsh scheme, in *The Representation of Cumulus Convection in Numerical Models*, *Meteorol. Monogr.*, vol. 24, pp. 165–170, edited by K. A. Emanuel and D. J. Raymond, Am. Meteorol. Soc., Boston, Mass.

Kaminski, J. W., et al. (2008), GEM-AQ, an on-line global multiscale chemical weather modelling system: Model description and evaluation of gas phase chemistry processes, *Atmos. Chem. Phys.*, *8*, 3255–3281, doi:10.5194/acp-8-3255-2008.

Karamchandani, P., Y. Zhang, S. Y. Chen, and R. Balmori-Bronson (2012), Development and testing of an extended chemical mechanism for global-through-urban applications, *Atmos. Pollut. Res.*, *3*(1), 1–24, doi:10.5094/APR.2011.047.

Keene, W. C., et al. (1999), Composite global emissions of reactive chlorine from anthropogenic and natural sources: Reactive chlorine emissions inventory, *J. Geophys. Res.*, *104*, 8429–8440, doi:10.1029/1998JD100084.

Kirner, O., R. Ruhnke, J. Buchholz-Dietsch, P. Jöckel, C. Brühl, and B. Steil (2011), Simulation of polar stratospheric clouds in the chemistry-climate-model EMAC via the submodel PSC, *Geosci. Model Dev.*, *4*, 169–182, doi:10.5194/gmd-4-169-2011.

Kulmala, M., K. Lehtinen, and A. Laaksonen (2006), Cluster activation theory as an explanation of the linear dependence between formation rate of 3 nm particles and sulphuric acid concentration, *Atmos. Chem. Phys.*, *6*, 787–793, doi:10.5194/acp-6-787-2006.

Langner, J., R. Bergstrom, and V. Foltescu (2005), Impact of climate change on surface ozone and deposition of sulphur and nitrogen in Europe, *Atmos. Environ.*, *39*, 1129–1141, doi:10.1016/j.atmosenv.2004.09.082.

Levis, S., C. Wiedinmyer, G. B. Bonan, and A. Guenther (2003), Simulating biogenic volatile organic compound emissions in the community climate system model, *J. Geophys. Res.*, *108*(D21), 4659, doi:10.1029/2002JD003203.

Liang, X.-Z., H. I. Choi, K. E. Kunkel, Y. Dai, E. Joseph, J. L. Wang, and P. Kumar (2005a), Development of the regional climate-weather research and forecasting (CWRF) model: Surface boundary conditions, Ill. State Water Surv., Champaign.

Liang, X.-Z., M. Xu, J. Zhu, K. E. Kunkel, and J. X. L. Wang (2005b), Development of the regional climate-weather research and forecasting model (CWRF): Treatment of topography, paper presented at 2005 Joint WRF/MM5 User's Workshop, Mesoscale and Microscale Meteorol. Div., Natl. Cent. for Atmos. Res., Boulder, Colo., 27–30 June.

Liao, H., and J. H. Seinfeld (2005), Global impacts of gas-phase chemistry-aerosol interactions on direct radiative forcing by anthropogenic aerosols and ozone, *J. Geophys. Res.*, *110*, D18208, doi:10.1029/2005JD005907.

Liao, H., Y. Zhang, W. T. Chen, F. Raes, and J. H. Seinfeld (2009), Effect of chemistry-aerosol-climate coupling on predictions of future climate and future levels of tropospheric ozone and aerosols, *J. Geophys. Res.*, *114*, D10306, doi:10.1029/2008JD010984.

Liao, K. J., E. Tagaris, K. Manomaiphiboon, C. Wang, J. H. Woo, P. Amar, S. He, and A. G. Russell (2009), Quantification of the impact of climate uncertainty on regional air quality, *Atmos. Chem. Phys.*, *9*, 865–878, doi:10.5194/acp-9-865-2009.

Lin, Y.-L., R. D. Farley, and H. D. Orville (1983), Bulk parameterization of the snow field in a cloud model, *J. Clim. Appl. Meteorol.*, *22*, 1065–1092, doi:10.1175/1520-0450(1983)022<1065:BPOTSF>2.0.CO;2.

Liu, Y., P. H. Daum, and R. L. McGraw (2005), Size truncation effect, threshold behavior, and a new type of autoconversion parameterization, *Geophys. Res. Lett.*, *32*, L11811, doi:10.1029/2005GL022636.

Liu, P., A. P. Tsimpidi, Y. Hu, B. Stone, A. G. Russell, and A. Nenes (2012), Differences between downscaling with spectral and grid nudging using WRF, *Atmos. Chem. Phys.*, *12*, 3601–3610, doi:10.5194/acp-12-3601-2012.

Liu, X.-H., Y. Zhang, S.-H. Cheng, J. Xing, Q. Zhang, D. G. Streets, C. J. Jang, W.-X. Wang, and J.-M. Hao (2010), Understanding of regional air pollution over China using CMAQ: Part I performance evaluation and seasonal variation, *Atmos. Environ.*, *44*(20), 2415–2426, doi:10.1016/j.atmosenv.2010.03.035.

Lohman, K., C. Seigneur, M. Gustin, and S. Lindberg (2008), Sensitivity of the global atmospheric cycle of mercury to emissions, *Appl. Geochem.*, *23*, 454–466, doi:10.1016/j.apgeochem.2007.12.022.

Marticorena, B., and G. Bergametti (1995), Modeling the atmospheric dust cycle: 1. Design of a soil-derived dust emission scheme, *J. Geophys. Res.*, *100*(D8), 16,415–16,430, doi:10.1029/95JD00690.

McCulloch, A., M. L. Aucott, C. M. Benkovitz, T. E. Graedel, G. Kleiman, P. M. Midgley, and Y.-F. Li (1999), Global emissions of hydrogen chloride and chloromethane from coal combustion, incineration, and industrial activities: Reactive chlorine emissions inventory, *J. Geophys. Res.*, *104*, 8391–8403, doi:10.1029/1999JD900025.

McMurry, P. H., and S. K. Friedlander (1979), New particle formation in the presence of an aerosol, *Atmos. Environ.*, *13*, 1635–1651, doi:10.1016/0004-6981(79)90322-6.

Mickley, L. J., D. J. Jacob, B. D. Field, and D. Rind (2004), Effects of future climate change on regional air pollution episodes in the United States, *Geophys. Res. Lett.*, *31*, L24103, doi:10.1029/2004GL021216.

Misenis, C., and Y. Zhang (2010), An examination of WRF/Chem: Physical parameterizations, nesting options, and grid resolutions, *Atmos. Res.*, *97*, 315–334, doi:10.1016/j.atmosres.2010.04.005.

Mlawer, E. J., S. J. Taubman, P. D. Brown, M. J. Iacono, and S. A. Clough (1997), Radiative transfer for inhomogeneous atmospheres: RRTM, a validated correlated-k model for the longwave, *J. Geophys. Res.*, *102*(D14), 16,663–16,682, doi:10.1029/97JD00237.

Monin, A. S., and A. M. Obukhov (1954), Basic laws of turbulent mixing in the surface layer of the atmosphere [in Russian], *Contrib. Geophys. Inst. Acad. Sci. USSR*, *151*, 163–187.

Neary, L., J. W. Kaminski, A. Lupu, and J. C. McConnell (2007), Developments and results from a Global Multiscale Air Quality Model (GEM-AQ), in *Air Pollution Modeling and Its Application XVII*, pp. 403–410, Springer, New York, doi:10.1007/978-0-387-68854-1_44.

Nenes, A., S. N. Pandis, and C. Pilinis (1998), ISORROPIA: A new thermodynamic equilibrium model for multiphase multicomponent inorganic aerosols, *Aquat. Geochem.*, *4*, 123–152, doi:10.1023/A:1009604003981.

O'Dowd, C. D., H. S. Michael, I. E. Consterdine, and J. A. Lowe (1997), Marine aerosol, sea-salt, and the marine sulphur cycle: A short review, *Atmos. Environ.*, *31*, 73–80, doi:10.1016/S1352-2310(96)00106-9.

Otkin, J. A., and T. J. Greenwald (2008), Comparison of WRF model-simulated and MODIS-derived cloud data, *Mon. Weather Rev.*, *136*, 1957–1970, doi:10.1175/2007MWR2293.1.

Pierce, T., C. Geron, L. Bender, R. Dennis, G. Tonnesen, and A. Guenther (1998), Influence of increased isoprene emissions on regional ozone modeling, *J. Geophys. Res.*, *103*(D19), 25,611–25,629, doi:10.1029/98JD01804.

Prather, M., et al. (2003), Fresh air in the 21st century?, *Geophys. Res. Lett.*, *30*(2), 1100, doi:10.1029/2002GL016285.

Pye, H. O. T., J. H. Seinfeld, H. Liao, S. Wu, L. J. Mickley, D. J. Jacob, and D. K. Henze (2009), Effect of changes in climate and emissions on future sulfate-nitrate-ammonium aerosol levels in the United States, *J. Geophys. Res.*, *114*, D01205, doi:10.1029/2008JD010701.

Ramanathan, V., et al. (2001), The Indian Ocean Experiment: An integrated assessment of the climate forcing and effects of the great Indo-Asian haze, *J. Geophys. Res.*, *106*(D22), 28,371–28,399.

Randall, D. A., et al. (2007), Climate models and their evaluation, in *Climate Change 2007: The Physical Science Basis. Contribution of Working Group I to the Fourth Assessment Report of the Intergovernmental Panel on Climate Change*, edited by S. Solomon et al., chap. 8, pp. 590–662, Cambridge Univ. Press, Cambridge, U. K.

Randerson, J. T., G. R. van der Werf, L. Giglio, G. J. Collatz, and P. S. Kasibhatla (2007), Global fire emissions database, version 2 (GFEDv2.1), http://daac.ornl.gov, Oak Ridge Natl. Lab. Distrib. Act. Arch. Cent., Oak Ridge, Tenn., doi:10.3334/ORNLDAAC/849.

Reiter, R. (1992), *Phenomena in Atmospheric and Environmental Electricity*, 505 pp., Elsevier, New York.

Richardson, M. I., A. D. Toigo, and C. E. Newman (2005), Non-conformal projection, global, and planetary versions of WRF, paper presented at

2005 Joint WRF/MM5 User's Workshop, Mesoscale and Microscale Meteorol. Div., Natl. Cent. for Atmos. Res., Boulder, Colo., 27–30 June.
Richardson, M. I., A. D. Toigo, and C. E. Newman (2007), PlanetWRF: A general purpose, local to global numerical model for planetary atmosphere and climate dynamics, *J. Geophys. Res.*, *112*, E09001, doi:10.1029/2006JE002825.
Roberts, G., M. J. Wooster, and E. Lagoudakis (2009), Annual and diurnal African biomass burning temporal dynamics, *Biogeosciences*, *6*, 849–866, doi:10.5194/bg-6-849-2009.
Roeckner, E., R. Brokopf, M. Esch, M. Giorgetta, S. Hagemann, L. Kornblueh, E. Manzini, U. Schlese, and U. Schulzweida (2006), Sensitivity of simulated climate to horizontal and vertical resolution in the ECHAM5 Atmosphere Model, *J. Clim.*, *19*, 3771–3791, doi:10.1175/JCLI3824.1.
Roy, B., R. Mathur, A. B. Gilliland, and S. C. Howard (2007), A comparison of CMAQ-based aerosol properties with IMPROVE, MODIS, and AERONET data, *J. Geophys. Res.*, *112*, D14301, doi:10.1029/2006JD008085.
Russell, A. G., and R. L. Dennis (2000), A NARSTO critical review of photochemical air quality modeling, *Atmos. Environ.*, *34*, 2283–2324, doi:10.1016/S1352-2310(99)00468-9.
Salzmann, M. (2008), WRF-Chem/KPP Coupler (WKC) for WRF V3, users' and developers guide v2.0, Princeton Univ., Princeton, N. J.
Sander, S. P., et al. (2006), Chemical kinetics and photochemical date for use in atmospheric studies, evaluation number 15, *Publ. 06-2*, Jet Propul. Lab., Pasadena, Calif.
Sanderson, M. G., W. J. Collins, C. E. Johnson, and R. G. Derwent (2006), Present and future acid deposition to ecosystems: The effect of climate change, *Atmos. Environ.*, *40*, 1275–1283, doi:10.1016/j.atmosenv.2005.10.031.
Sarwar, G., D. Luecken, G. Yarwood, G. Whitten, and W. P. L. Carter (2008), Impact of an updated carbon bond mechanism on predictions from the Community Multiscale Air Quality Model, *J. Appl. Meteorol. Climatol.*, *47*, 3–14, doi:10.1175/2007JAMC1393.1.
Schell, B., I. J. Ackermann, H. Hass, F. S. Binkowski, and A. Ebel (2001), Modeling the formation of secondary organic aerosol within a comprehensive air quality modeling system, *J. Geophys. Res.*, *106*, 28,275–28,293, doi:10.1029/2001JD000384.
Schultz, M., et al. (2007), Emission datasets and methodologies for estimating emissions, *RETRO Rep., D1-6*, Fifth Framework Programme, Eur. Comm., Brussels. [Available at http://retro.enes.org]
Seigneur, C., P. Karamchandani, K. Lohman, K. Vijayaraghavan, and R.-L. Shia (2001), Multiscale modeling of the atmospheric fate and transport of mercury, *J. Geophys. Res.*, *106*, 27,795–27,809, doi:10.1029/2000JD000273.
Seigneur, C., K. Vijayaraghavan, K. Lohman, P. Karamchandani, and C. Scott (2004), Global source attribution for mercury deposition in the United States, *Environ. Sci. Technol.*, *38*, 555–569, doi:10.1021/es034109t.
Seinfeld, J. H. (2004), Air pollution: A half century of progress, *AIChE J.*, *50*(6), 1096–1108, doi:10.1002/aic.10102.
Seinfeld, J. H., and S. N. Pandis (2006), *Atmospheric Chemistry and Physics: From Air Pollution to Climate Change*, 2nd ed., 1232 pp., John Wiley, New York, doi:10.1063/1.882420.
Shaw, P. (2008), Application of aerosol speciation data as an in situ dust proxy for validation of the Dust Regional Atmospheric Model (DREAM), *Atmos. Environ.*, *42*, 7304–7309, doi:10.1016/j.atmosenv.2008.06.018.
Sihto, S., M. Kulmala, V. Kerminen, M. Dal Maso, T. Petäjä, I. Riipinen, H. Korhonen, F. Arnold, R. Janson, and M. Boy (2006), Atmospheric sulphuric acid and aerosol formation: Implications from atmospheric measurements for nucleation and early growth mechanisms, *Atmos. Chem. Phys.*, *6*, 4079–4091, doi:10.5194/acp-6-4079-2006.
Simpson, D., A. Guenther, C. N. Hewitt, and R. Steinbreche (1995), Biogenic emissions in Europe: 1. Estimates and uncertainties, *J. Geophys. Res.*, *100*(D11), 22,875–22,890, doi:10.1029/95JD02368.
Skamarock, W. C., J. B. Klemp, J. Dudhia, D. O. Gill, D. M. Barker, M. G. Duda, X.-Y. Huang, W. Wang, and J. G. Powers (2008), A description of the Advanced Research WRF version 3, *Tech. Note, NCAR/TN-475+STR*, Natl. Cent. for Atmos. Res., Boulder, Colo. [Available at http://www.mmm.ucar.edu/wrf/users/docs/arw_v3.pdf]
Stockwell, W. R., P. Middleton, J. S. Chang, and X. Tang (1990), The second generation regional acid deposition model chemical mechanism for regional air quality modeling, *J. Geophys. Res.*, *95*, 16,343–16,367, doi:10.1029/JD095iD10p16343.
Stockwell, W. R., F. Kirchner, M. Kuhn, and S. Seefeld (1997), A new mechanism for regional atmospheric chemistry modeling, *J. Geophys. Res.*, *102*, 25,847–25,879, doi:10.1029/97JD00849.
Streets, D. G., et al. (2003), An inventory of gaseous and primary aerosol emissions in Asia in the year 2000, *J. Geophys. Res.*, *108*(D21), 8809, doi:10.1029/2002JD003093.
Streets, D. G., Q. Zhang, L. Wang, K. He, J. Hao, Y. Wu, Y. Tang, and G. R. Carmichael (2006), Revisiting China's CO emissions after TRACE-P: Synthesis of inventories, atmospheric modeling, and observations, *J. Geophys. Res.*, *111*, D14306, doi:10.1029/2006JD007118.
Tagaris, E., K. Manomaiphiboon, K.-J. Liao, L. R. Leung, J.-H. Woo, S. He, P. Amar, and A. G. Russell (2007), Impacts of global climate change and emissions on regional ozone and fine particulate matter concentrations over the United States, *J. Geophys. Res.*, *112*, D14312, doi:10.1029/2006JD008262.
Tie, X., S. Madronich, S. Walters, R. Zhang, P. Rasch, and W. Collins (2003), Effect of clouds on photolysis and oxidants in the troposphere, *J. Geophys. Res.*, *108*(D20), 4642, doi:10.1029/2003JD003659.
Uno, I., et al. (2003), Regional chemical weather forecasting system CFORS: Model descriptions and analysis of surface observations at Japanese island stations during the ACE-Asia experiment, *J. Geophys. Res.*, *108*(D23), 8668, doi:10.1029/2002JD002845.
Usoskin, I. G., and G. A. Kovaltsov (2006), Cosmic ray induced ionization in the atmosphere: Full modeling and practical applications, *J. Geophys. Res.*, *111*, D21206, doi:10.1029/2006JD007150.
Wang, H., W. C. Skamarock, and G. Feingold (2009), Evaluation of scalar advection schemes in the Advanced Research WRF model using large-eddy simulations of aerosol-cloud interactions, *Mon. Weather Rev.*, *137*, 2547–2558, doi:10.1175/2009MWR2820.1.
Wang, H., G. Feingold, R. Wood, and J. Kazil (2010), Modelling microphysical and meteorological controls on precipitation and cloud cellular structures in Southeast Pacific stratocumulus, *Atmos. Chem. Phys.*, *10*, 6347–6362.
Wang, K., Y. Zhang, C. J. Jang, S. Phillips, and B.-Y. Wang (2009), Modeling study of intercontinental air pollution transport over the Trans-Pacific Region in 2001 using the Community Multiscale Air Quality Modeling System, *J. Geophys. Res.*, *114*, D04307, doi:10.1029/2008JD010807.
Wang, L.-T., et al. (2010), Assessment of air quality benefits from national air pollution control policies in China. I: Background, emission scenarios and evaluation of meteorological predictions, *Atmos. Environ.*, *44*(28), 3442–3448, doi:10.1016/j.atmosenv.2010.05.051.
Weaver, C. P., et al. (2009), A preliminary synthesis of modeled climate change impacts on US regional ozone concentrations, *Bull. Am. Meteorol. Soc.*, *90*, 1843–1863, doi:10.1175/2009BAMS2568.1.
Yarwood, G., S. Rao, M. Yocke, and G. Z. Whitten (2005), Updates to the carbon bond mechanism: CB05, report, ENVIRON Int. Corp., Novato, Calif. [Available at http://www.camx.com/publications/model-development.aspx/]
Yu, F. (2006), From molecular clusters to nanoparticles: Second-generation ion-mediated nucleation model, *Atmos. Chem. Phys.*, *6*, 5193–5211, doi:10.5194/acp-6-5193-2006.
Yu, F. (2010), Ion-mediated nucleation in the atmosphere: Key controlling parameters, implications, and look-up table, *J. Geophys. Res.*, *115*, D03206, doi:10.1029/2009JD012630.
Yu, F., and G. Luo (2009), Simulation of particle size distribution with a global aerosol model: Contribution of nucleation to aerosol and CCN number concentrations, *Atmos. Chem. Phys.*, *9*, 7691–7710, doi:10.5194/acp-9-7691-2009.
Yu, F., and R. P. Turco (2000), Ultrafine aerosol formation via ion-mediated nucleation, *Geophys. Res. Lett.*, *27*, 883–886, doi:10.1029/1999GL011151.
Yu, F., and R. P. Turco (2011), The size-dependent charge fraction of sub-3-nm particles as a key diagnostic of competitive nucleation mechanisms under atmospheric conditions, *Atmos. Chem. Phys.*, *11*, 9451–9463, doi:10.5194/acp-11-9451-2011.
Yu, F., Z. Wang, G. Luo, and R. P. Turco (2008), Ion-mediated nucleation as an important source of tropospheric aerosols, *Atmos. Chem. Phys.*, *8*, 2537–2554, doi:10.5194/acp-8-2537-2008.
Yu, F., G. Luo, T. Bates, B. Anderson, A. Clarke, V. Kapustin, R. Yantosca, Y. Wang, and S. Wu (2010), Spatial distributions of particle number concentrations in the global troposphere: Simulations, observations, and implications for nucleation mechanisms, *J. Geophys. Res.*, *115*, D17205, doi:10.1029/2009JD013473.
Yu, S.-C., R. Mathur, J. Pleim, D. Wong, A. G. Carlton, S. Roselle, and S. T. Rao (2011), Simulation of the indirect radiative forcing of climate due to aerosols by the two-way coupled WRF-CMAQ over the eastern United States, in *Air Pollution Modeling and Its Applications XXI*, edited by D. G. Steyn and S. Trini Castelli, chap. 96, pp. 579–583, Springer, Dordrecht, Netherlands.
Zaveri, R. A., and L. K. Peters (1999), A new lumped structure photochemical mechanism for large-scale applications, *J. Geophys. Res.*, *104*, 30,387–30,415.

Zaveri, R. A., R. C. Easter, J. D. Fast, and L. K. Peters (2008), Model for Simulating Aerosol Interactions and Chemistry (MOSAIC), *J. Geophys. Res.*, *113*, D13204, doi:10.1029/2007JD008782.

Zender, C. S., H. Bian, and D. Newman (2003), Mineral Dust Entrainment and Deposition (DEAD) model: Description and 1990s dust climatology, *J. Geophys. Res.*, *108*(D14), 4416, doi:10.1029/2002JD002775.

Zhang, Q., et al. (2009), Asian emissions in 2006 for the NASA INTEX-B mission, *Atmos. Chem. Phys.*, *9*, 5131–5153, doi:10.5194/acp-9-5131-2009.

Zhang, Y. (2008), Online coupled meteorology and chemistry models: History, current status, and outlook, *Atmos. Chem. Phys.*, *8*, 2895–2932, doi:10.5194/acp-8-2895-2008.

Zhang, Y., B. Pun, K. Vijayaraghavan, S.-Y. Wu, C. Seigneur, S. Pandis, M. Jacobson, A. Nenes, and J. H. Seinfeld (2004), Development and application of the Model of Aerosol Dynamics, Reaction, Ionization and Dissolution (MADRID), *J. Geophys. Res.*, *109*, D01202, doi:10.1029/2003JD003501.

Zhang, Y., K. Vijayaraghavan, X.-Y. Wen, H. E. Snell, and M. Z. Jacobson (2009a), Probing into regional ozone and particulate matter pollution in the United States: 1. A 1-year CMAQ simulation and evaluation using surface and satellite data, *J. Geophys. Res.*, *114*, D22304, doi:10.1029/2009JD011898.

Zhang, Y., X.-Y. Wen, K. Wang, K. Vijayaraghavan, and M. Z. Jacobson (2009b), Probing into regional ozone and particulate matter pollution in the United States: 2. An examination of formation mechanisms through a process analysis technique and sensitivity study, *J. Geophys. Res.*, *114*, D22305, doi:10.1029/2009JD011900.

Zhang, Y., X.-Y. Wen, and C. J. Jang (2010a), Simulating climate-chemistry-aerosol-cloud-radiation feedbacks in continental U.S. using online-coupled WRF/Chem, *Atmos. Environ.*, *44*(29), 3568–3582, doi:10.1016/j.atmosenv.2010.05.056.

Zhang, Y., Y. Pan, K. Wang, J. D. Fast, and G. A. Grell (2010b), WRF/Chem-MADRID: Incorporation of an aerosol module into WRF/Chem and its initial application to the TexAQS2000 episode, *J. Geophys. Res.*, *115*, D18202, doi:10.1029/2009JD013443.

Zhang, Y., Y.-C. Chen, G. Sarwar, and K. Schere (2012a), Impact of gas-phase mechanisms on WRF/Chem predictions: Mechanism implementation and comparative evaluation, *J. Geophys. Res.*, *117*, D01301, doi:10.1029/2011JD015775.

Zhang, Y., J. Hemperly, N. Meskhidze, and W. C. Skamarock (2012b), The Global Weather Research and Forecasting (GWRF) Model: Model evaluation, sensitivity study, and future year simulation, *Atmos. Clim. Sci.*, *2*(3), 231–253, doi:10.4236/acs.2012.23024.